

1. INTRODUCTION

1.1 Inspiration for this Project

Surface modification with self-assembled monolayers. A self-assembled monolayer (SAM) constitutes organic molecules that align on the surface of a substrate in regular arrays.¹⁻³ These molecules are distinguished by their capability of attaching to a solid surface via energetically favorable interactions. They adsorb to the surface of interest from a solution or vapor phase to form a densely packed molecular barrier on a substrate.³ The interactions between these molecules and the surface utilize a variety of intermolecular forces such as hydrogen bonding, electrostatic attractions, and covalent bonding. As a result, the design and preparation of SAMs are extremely flexible in terms of materials and reaction conditions.

The field of SAMs has experienced enormous development since Zisman *et al.* published a paper on adsorbing an n-alkyl amine-based surfactant to a metal surface in 1946,⁴ initiating the concept of self-assembly. The recent boom in nanotechnology has further accelerated the progress of this field. Indeed, SAMs are nanostructure in nature.³ They are frequently applied as model substrates in research for electrode modification,⁵ corrosion protection of metals,⁶ synthesis of fullerene and chromophoric films,^{7,8} and preparation of biocompatible materials.⁹ The great versatility of these surface coatings is primarily attributed to the patterned structures of the molecular assemblies, which introduce novel chemical

and physical properties to their substrates, activating them for further modifications.

Although self-assembly of molecules has been exploited by a wide range of applications, more efforts must be focused on improving the control of the growth process to tailor the orientation and dynamics of these molecules for a specific purpose. This project was initiated as an attempt to investigate the fundamental issues in the preparation of SAMs by reacting aminosilanes with the native oxide layer (silica) on smooth silicon wafers.

Amine-terminated films. Amine-terminated organic molecules are frequently used to construct SAMs with their primary amine moieties exposed to the exterior. These organic films are anchored to solid surfaces via specific and stable interactions without involving their amine moieties. For instance, 3-aminopropylalkoxysilane attaches to a silica surface via siloxane bonds, Si-O-Si, to form an amine-terminated surface that can be used to immobilize enzymes and other materials.^{10, 11} In general, an amine-terminated organic film with a horizontal array of primary amine moieties available for further derivatizations is ideal for many applications.

Alkoxy-based silane molecules with the general formula $\text{NH}_2\text{-(CH}_2\text{)}_k\text{-Si(OR)}_3$ are silane coupling agents commonly used to activate silica surfaces through a reaction, known as silanization. One of the most typical modification processes involves depositing 3-aminopropyltriethoxysilane (APTES) on silicon wafers,¹²⁻¹⁷ which can be then used to graft different organic molecules such as

poly(ethylene glycol).¹⁶ The multi-functionality of APTES allows it to be attached to an inorganic silica surface in a closely packed array via stable covalent siloxane bonds through its three alkoxy groups while maintaining the free amine group for further modifications.

In this project, the behaviors of APTES in both solution-phase and vapor-phase silanization on silicon wafers were analyzed and used as the basis for evaluating the performances of four other commercially available silane coupling agents.

Surface morphology and hydrolytic stability of SAMs. The homogeneity in surface morphology of SAMs is critical for most research and applications. For instance, DNA immobilized on flat APTES-coated mica surface can only be imaged properly with atomic force microscopy (AFM) when the amine-terminated background has a roughness lower than that of the DNA.¹⁸ Smooth SAMs are also essential for adhesion studies since the homogeneity of functional layers affect the specificity and sensitivity of the substrates to their analytes, which can be either chemicals or microorganisms.¹⁹⁻²¹

The hydrolytic stability of SAMs is another important consideration. When the aminosilane-coated substrates are used for grafting hydrophilic polymers such as dextrans, they are exposed to an aqueous environment for up to 96 h.²² A hydrolytically stable SAM is therefore crucial for effective grafting of biologically and environmentally relevant molecules onto inorganic substrates.

In this project, the surface morphology of aminosilane-derived layers on silicon wafers was analyzed with AFM and contact angle goniometry. The hydrolytic stability of these organic layers prepared under different conditions was studied as a function of their thickness against time.

1.2 Background Information

Mechanism of silanization. The covalent attachment of an aminosilane molecule to a silica surface proceeds in two steps (Figure 1a). The first step begins with the hydrolysis of an aminosilane molecule via an S_N2 exchange of an alkoxy group for a hydroxyl group. The second step involves the condensation of a water molecule, resulting in the formation of a siloxane bond, covalent in nature.

The amine groups can catalyze the siloxane bond formation both intramolecularly and inter-molecularly.²³ Intra-molecular catalysis (Figure 1b) is initiated by the amine group coordinating to the silicon atom of the same molecule via the formation of a penta-coordinated cyclic intermediate, facilitating the covalent attachment of an aminosilane molecule to a silica surface. Inter-molecular catalysis (Figure 1c) involves the amine group of an aminosilane molecule coordinating to the silicon atom of another aminosilane molecule in close proximity.

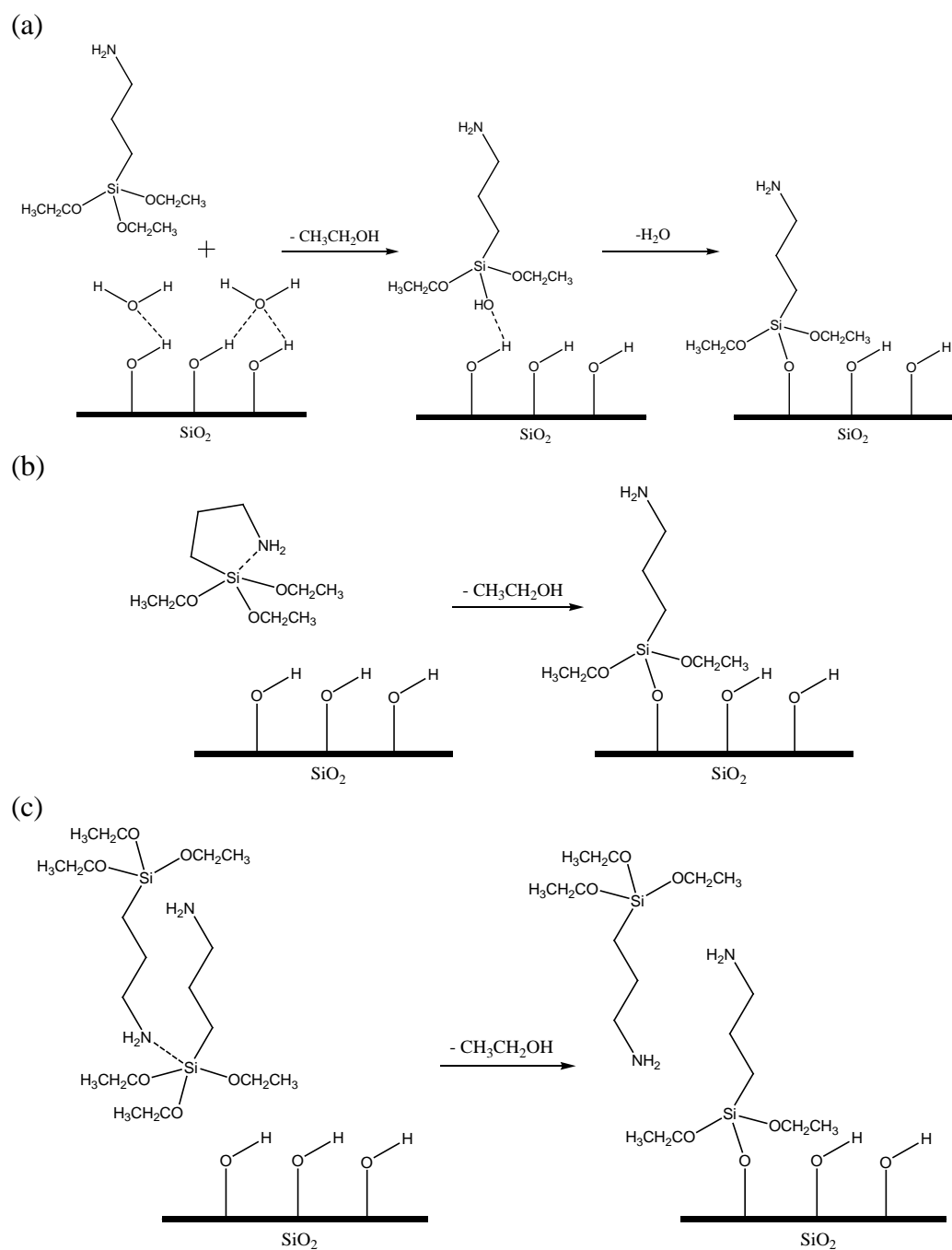


Figure 1. Covalent attachment of 3-aminopropyltriethoxysilane to a silica surface: (a) basic mechanism of silanization, (b) intra-molecular catalysis by amine, and (c) inter-molecular catalysis by amine.

Conformations of aminosilane. The conformations of trialkoxy aminosilane on a silica surface depend on the density of aminosilane molecules and the type of bonding.²³ When an aminosilane molecule is covalently attached to a silica surface via a siloxane bond, it can have an upright conformation (Figure 2a) or a tilted one (Figure 2b) due to the attraction between its terminal amine and the proton on the silanol oxygen.

The aminosilane molecules are also capable of cross-linking with one another both vertically and horizontally, giving rise to multilayers (Figure 3a, vertical polymerization) in addition to dense monolayers (Figure 3b, horizontal polymerization).²⁴ The type and extent of cross-linking is particularly sensitive to water content in a reaction and thus reduces the reproducibility of this type of modification process.

In addition, the possibility of aminosilane molecules to be physisorbed to a silica surface via hydrogen bonding limits the stability of silane derived layers since physisorbed molecules are easily removed from the surface by rinsing in water (Figure 2c-e).²⁵ In this study, the modified substrates were rinsed rigorously in toluene, ethanol, and water to remove loosely attached molecules before characterization. The variable surface conformations of aminosilanes make it a challenging task to produce high-density and stable SAMs on substrates.

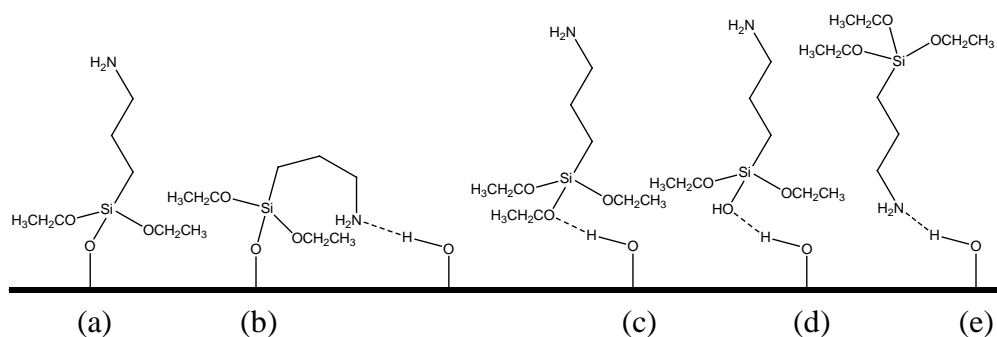


Figure 2. Possible conformations of 3-aminopropyltriethoxysilane on a silica surface.

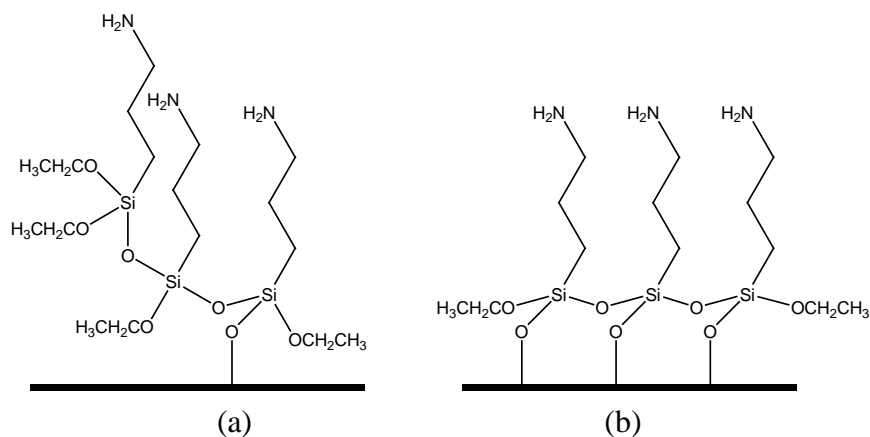


Figure 3. Polymerization of 3-aminopropyltriethoxysilane on a silica surface: (a) vertical and (b) horizontal.

Hydrolytic stability of aminosilane-derived layers. Degradations of aminosilane-derived layers were observed when modified substrates were exposed to an aqueous medium for an extensive period of time.²³ The loss of thickness is proposed to mainly occur through the hydrolysis of siloxane bonds between aminosilane molecules and silica surfaces.²³ Shown in Figure 4, water attacks the silicon atom via an S_N2 reaction and this process can also be catalyzed by the amine groups intra- and inter-molecularly similar to the catalysis of a

siloxane bond formation. Amine groups can catalyze the formation and the degradation of siloxane bonds between aminosilane-derived layers and silicon wafer substrates. The main goal of this study is to look for aminosilanes and reaction conditions that promote the formation but discourage the degradation of siloxane bonds.

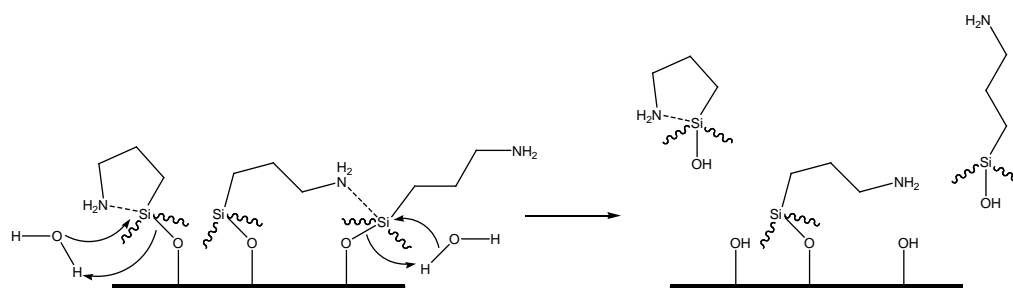


Figure 4. *Intra- and inter-molecular catalysis of the hydrolysis of siloxane bonds between 3-aminopropyltriethoxysilane and a silica surface.*

Choice of reagents. Tri-alkoxy aminosilanes were chosen over mono- and di-alkoxy aminosilanes for their capability of forming multiple siloxane bonds with a substrate and neighboring silane molecules as shown in Figure 5, giving rise to enhanced hydrolytic stability.

A total of five silane coupling agents – APTES, 3-aminopropyltrimethoxysilane (APTMS), N-(6-aminohexyl)aminomethyltriethoxysilane (AHAMTES), N-(2-aminoethyl)-3-aminopropyltriethoxysilane (AEAPTES), and N-(2-aminoethyl)-3-aminopropyltrimethoxysilane (AEAPTMS) – were analyzed in both solution-phase and vapor-phase silanization reactions for their hydrolytic stability on silicon wafers.

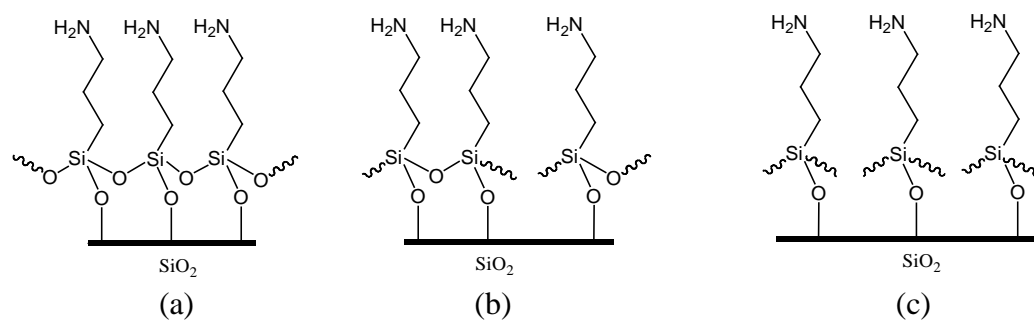


Figure 5. SAMs derived with (a) tri-alkoxy aminosilane, (b) di-alkoxy aminosilane, and (c) mono-alkoxy aminosilane.

1.3 Foundation Work

General challenges. The complex binding mechanisms between silane coupling agents and silicon wafers have prompted many studies to investigate the impact of varying reaction conditions on the covalent attachment of aminosilanes and their conformations on substrates. Generally, critical reaction parameters include reaction time, temperature, silane concentration, rinsing protocol, drying and curing methods. Furthermore, silanization's acute sensitivity to water complicates the experimental design. Although most studies reported in the literature focused on analyzing only one aspect of the reaction and their results showed poor consistencies with one another, some consensuses have been recognized. For instance, submerging silicon wafers in piranha solution (7 parts concentrated sulfuric acid and 3 parts 30% hydrogen peroxide) and subsequent rinsing in water are known to maximize silanol groups on silicon wafers,^{26,27} which are essential for the formation of siloxane bonds. Reaction parameters that are critical to the preparation and stability of SAMs of aminosilanes are discussed in the subsequent sections.

Solution-phase silanization. A solution-phase silanization reaction is usually carried out by submerging silicon wafers in an aminosilane solution for a desired amount of time. This method is often used by biologists for its ease of preparing relatively thick aminosilane-derived layers, however, homogeneous surface morphologies and hydrolytic stability of the silane layers are compromised due to the lack of control over the growth process. Specifically, the following issues need to be considered.

First, the nature of solvent affects the solubility of a silane coupling agent and the amount of water present in the reaction. Non-polar organic solvents are generally suitable for silanization since they readily dissolve aminosilanes and have low capacity for dissolving water. In the complete absence of water, alkoxy groups cannot be hydrolyzed and silanization solely relies on the amine moieties for catalysis, resulting in disordered SAMs with low primary amine contents.²⁶ Excess water, however, leads to uncontrollable polymerization in both horizontal and vertical directions, giving rise to extremely thick and rough multilayers. As a result, only a trace amount of water is required for silanization.^{28, 29} Anhydrous toluene that dissolves aminosilanes and contains a very small amount of water meets these requirements.

Secondly, the purity of a silane coupling agent and its concentration in the reaction medium affect the surface morphology and the hydrolytic stability of aminosilane-derived layers. Impurities in an aminosilane reagent may exist in the form of oligomers and polymers of aminosilane molecules, which may be

introduced during the manufacturing and storage process. A higher silane concentration in the reaction medium increases the chances of aminosilane molecules reacting with each other and forming aggregates in solution. The aggregates existing as impurities in a silane coupling agent and those formed during silanization are variable in size. Their depositions on a substrate disrupt the regular arrays of aminosilane molecules, creating structural defects susceptible to water penetration. Additionally, these aggregates could be attached to a substrate via very few siloxane bonds and hence easily removed by hydrolysis. As a result, high silane purity and low solution concentration promote the formation of silane layers with uniform morphologies. Based on previous studies,^{23, 26} 0.5 mL and 1.0 mL of a silane coupling agent in 25 mL of anhydrous toluene were chosen for solution-phase silanization. The silane layers prepared at these two concentrations presented little differences and therefore the lower concentration was adopted throughout this study.

Thirdly, reaction time and temperature also affect the quality of aminosilane-derived layers. Extending reaction time allows the formation of thick multilayers at the expense of structural regularity because horizontal and vertical polymerizations compete with each other. Raising reaction temperature increases the reaction rate and results in greater chances of aggregation as aminosilane molecules collide with one another more frequently in the reaction medium. These aggregates introduce rough surface features as they are deposited on a substrate. In addition, high costs associated with extensive reaction time and high

reaction temperatures are not desirable. Thus, moderate reaction time and temperature that generate considerably thick and stable aminosilane-derived layers are targeted. Previous research has shown that silanization in anhydrous toluene at ~ 70 °C for 24 h produces aminosilane-derived layers with appreciable thickness and homogeneous surface morphologies.^{23, 30}

Furthermore, curing samples at a temperature slightly higher than 100 °C after silanization is reported to increase the primary amine contents by promoting condensation of water and thermally inducing breakage of hydrogen bonds that liberate amine groups from negatively charged silica surfaces.^{23, 26, 31} However, an excessively high curing temperature should be avoided since amine groups may be consumed by reacting with atmospheric carbon dioxide to form carbamate.²⁶

Vapor-phase silanization. Vapor-phase reactions have been developed to improve the control of the SAM growth process. Compared to solution-phase reactions, vapor-phase reactions greatly simplify the experimental design. First of all, they eliminate the impact of silane purity since impurities in the form of oligomers and polymers do not vaporize easily and hence do not react with the substrate. Secondly, vapor-phase reactions are usually in the absence of a solvent and therefore confer a better control of the amount of water present in a reaction, minimizing the occurrence of aggregation. Thirdly, they simplify post-silanization rinsing of substrates.

The major drawback of this approach is the unknown nature of bonding between the silane and the silica surface. Consequently, evaluating the hydrolytic

stability of aminosilane-derived layers is particularly important for vapor-phase reactions.

Multiple studies were reported in the literature to demonstrate the feasibility of vapor-phase silanization.³³⁻³⁷ More efforts, however, need to be focused on optimizing the reaction conditions, which were rigorously pursued in this study.

Other considerations. Although the capability of an aminosilane molecule to covalently attach to a silica surface has been generally accepted, the nature of their interactions is not clear. Recent studies attempted to analyze the nature of bonding via Fourier transform-infrared spectroscopy (FT-IR).^{32, 38} It was reported that solution-phase reactions at room temperature give rise to siloxane bond formation at the interface between a silane coupling agent and a silica surface. However, vapor-phase reactions at elevated temperatures do not directly lead to siloxane bond formation, which can be induced subsequently by submerging modified substrates in water. Our post-silanization treatments such as the rinsing and drying of substrates were aimed to promote siloxane bond formation.

1.4 Objectives

Hypothesis. We aimed to enhance the hydrolytic stability of aminosilane-derived layers by optimizing reaction conditions to increase the density of aminosilane molecules on silicon wafers. Densely packed aminosilane molecules would minimize amine-catalyzed hydrolysis of siloxane bonds. We also evaluated the performances of five different silane coupling agents with variable chain

lengths in both solution- and vapor-phase silanization. Longer chains would increase the steric hindrance to the bending of aminosilane molecules and therefore reduce the catalysis of siloxane bond breakage by amine groups.

Based on their molecular structures, we categorized these five silane coupling agents into three groups (Table 1). Group I reagents, including APTES and APTMS, contain a primary amine group at propyl or butyl position. They are capable of catalyzing the formation and hydrolysis of siloxane bonds both intra- and inter-molecularly. Intra-molecular catalysis is achieved via the formation of stable five- or six-membered cyclic intermediates. Group II reagents, including AEAPTES and AEAPTMS, contain a secondary amine group at propyl or butyl position. Similar to Group I reagents, they are capable of intra- and inter-molecular catalysis, however, due to the steric hindrance imposed by their longer chains, amine-catalyzed hydrolysis of siloxane bonds would be reduced. Group III reagents, including AHAMTES, do not have any amine group at propyl or butyl position. As a result, they are only capable of inter-molecular catalysis.

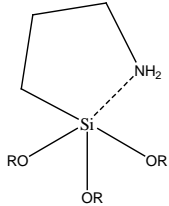
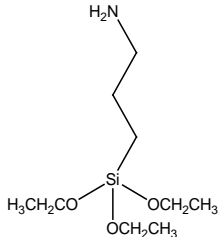
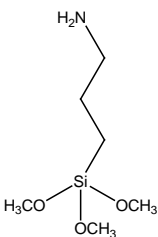
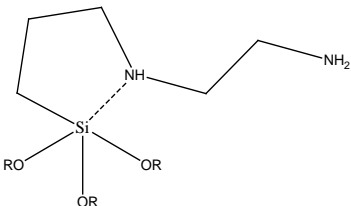
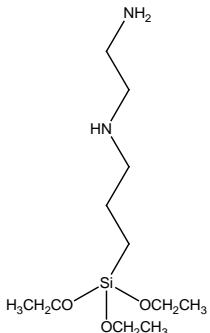
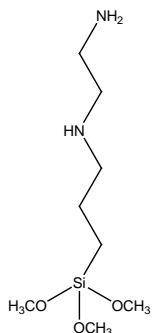
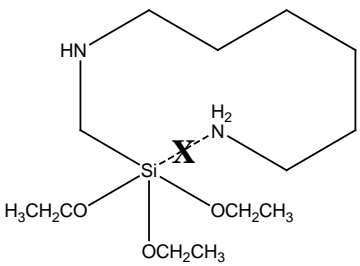
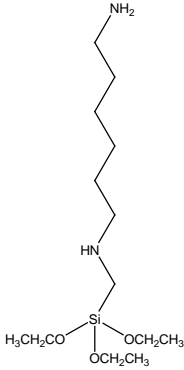
Experimental design. Solution-phase silanization was carried out in anhydrous toluene at 70 °C for either 24 h or 48 h and vapor-phase silanization was carried out mostly at 90 °C for either 24 h or 48 h. Silane coupling agents were used as received from Gelest without further purification. All the samples were cured at 110 °C post silanization. The hydrolytic stability of aminosilane-derived layers was studied as a function of time by submerging the samples in Milli-Q water at 40 °C for different amounts of time up to 48 h. The temperature,

40 °C, was chosen to simulate biological media in a slightly accelerated manner.

Modified substrates were characterized to acquire information about their

thickness, wettability, surface composition, and surface topography.

Table 1. Three groups of silane coupling agents.

Group	Reagent(s)	
 <p data-bbox="467 789 737 852">I. Primary amine can coordinate to Si</p>	 <p data-bbox="943 821 1052 852">APTES</p>	 <p data-bbox="1214 821 1323 852">APTMS</p>
 <p data-bbox="443 1129 760 1192">II. Secondary amine can coordinate to Si</p>	 <p data-bbox="911 1209 1060 1241">AEAPTES</p>	 <p data-bbox="1195 1209 1349 1241">AEAPTMS</p>
 <p data-bbox="410 1583 792 1646">III. No amine can coordinate to Si</p>	 <p data-bbox="1040 1656 1195 1688">AHAMTES</p>	

2. EXPERIMENTAL

2.1 Materials and Apparati

General. Silicon wafers (100 orientation, P/B doped, resistivity 1–10 Ω -cm, thickness 475–575 μ m) were purchased from International Wafer Service, Inc. (USA). Silane coupling agents, including 3-aminopropyltriethoxysilane (APTES, 99.7% pure), 3-aminopropyltrimethoxysilane (APTMS, 98.5% pure), N-(6-aminohexyl)aminomethyltriethoxysilane (AHAMTES, 99.66% pure), N-(2-aminoethyl)-3-aminopropyltriethoxysilane (AEAPTES, 97.4% pure), and N-(2-aminoethyl)-3-aminopropyltrimethoxysilane (AEAPTMS, 98.3% pure), were purchased from Gelest, Inc. (USA). They were stored under nitrogen and used without further distillation. House-purified water (reverse osmosis) was purified in a Millipore Milli-Q Biocell System (Millipore Corp., USA) that involved reverse osmosis, ion exchange, and filtration (18.2 M Ω -cm). Other reagents were used as received from Thermo Fisher Scientific, Inc. (USA). Solution-phase silanization was carried out in anhydrous toluene that was dried and deoxygenated through a Pure Solv 400-6 solvent purification system (Innovative Technology, Inc., USA). All glassware was cleaned in a base bath (potassium hydroxide and isopropyl alcohol), rinsed with distilled water (3 \times), and stored in a clean oven at 110 $^{\circ}$ C until use.

Instrumentation. Thicknesses of aminosilane-derived layers were measured with a LSE Stokes Ellipsometer (Gaertner Scientific Corp., USA).

Contact angles were measured with a NRL C.A. 100-00 goniometer (ramé-hart Instrument Co., USA) with a Gilmont syringe (Gilmont Instrument Co., USA) and a 24-gauge flat-tipped needle. Atomic force microscope images were obtained with a Veeco Metrology Dimension 3100 Atomic Force Microscope (Veeco Instruments, Inc., USA) under tapping mode with a Veeco silicon tip (resistivity 1–10 Ω -cm, P doped). Roughness of surface features was determined using the Nanoscope software (Veeco Instruments, Inc., USA). Atomic compositions (C, O, Si, and N contents) of the surfaces were analyzed by X-ray photoelectron spectroscopy using a Quantum 2000 Scanning ESCA Microprobe (Physical Electronics, Inc., USA). Thermo NESLAB heated baths (Thermo Fisher Scientific, Inc., USA) were used to maintain the temperatures for silanization reactions and tests for hydrolytic stability. Precision 51221126 Gravity Convection Lab Oven (Thermo Fisher Scientific, Inc., USA) was used for storing clean glassware and drying clean and silanized silicon wafers.

2.2 Methods

Preparation of silicon wafers. Silicon wafers were cut into rectangular pieces (1.2×1.5 cm), rinsed with house-purified water, and dried with compressed air. They were then placed in a custom-designed glass holder and cleaned by submerging in a freshly prepared piranha solution containing 7 parts concentrated sulfuric acid and 3 parts 30% hydrogen peroxide for 45 min. After

being removed from the solution, wafers were rinsed with copious amounts of water and dried in a clean oven at 110 °C for 30 min.

Solution-phase silanization. Clean wafers were transferred to a clean glass holder, placed in a custom-designed Schlenk tube (inner diameter 2.5 cm) fitted with an o-ring joint and a Teflon stopcock (ACE Glass, Inc., USA). Using the Pure Solv system, the tube was flushed with nitrogen and evacuated (3 ×) before 25 mL of anhydrous toluene was dispensed. Under nitrogen, 0.5 mL of an aminosilane reagent was cannulated into the reaction tube while the solution was being stirred. Reactions were carried out at 70 °C in an oil bath for desired amounts of time. After silanization, the wafers were individually rinsed in toluene (2 ×), ethanol (2 ×) and water (2 ×), and dried in an oven at 110 °C for 15 min. Thickness and contact angle measurements were carried out immediately upon cooling for ~5 min.

Vapor-phase silanization. Clean wafers were transferred to a clean glass holder, placed in a custom-designed Schlenk tube fitted with an o-ring joint and a Teflon stopcock. After purging the system with nitrogen for ~30 min, 0.5 mL of an aminosilane reagent was cannulated into the reaction tube under nitrogen. Reactions were carried out at 70 °C, 90 °C, 100 °C, or 105 °C in an oil bath for desired amounts of time. After silanization, the wafers were rinsed individually with toluene (2 ×), ethanol (2 ×) and water (2 ×), and dried in an oven at 110 °C

for 15 min. Thickness and contact angle measurements were carried out immediately upon cooling for ~5 min.

Test method for hydrolytic stability. Freshly silanized samples were placed in a clean glass holder and submerged in Milli-Q water in a tightly closed Schlenk tube at 40 °C for 1 h, 3 h, 12 h, 24 h, or 48 h. Samples were then rinsed in distilled water and dried in an oven at 110 °C for 15 min before characterization.

3. SURFACE CHARACTERIZATION TECHNIQUES

3.1 Ellipsometry

General. Ellipsometry measures the changes in polarization of elliptically polarized light upon its reflection from a surface. It yields information about the thickness and optical properties of the characterized surface. In this study, ellipsometry was adopted to measure the thickness of aminosilane-derived layers, ranging from ~ 2 Å to ~ 500 Å. The thickness of a clean silicon wafer substrate and that of the modified substrate were respectively measured before and after silanization. Hence, the thickness of the aminosilane-derived layer was estimated to be the difference between these two measurements.

Theory. Light is an electromagnetic transverse wave composing of an electric field and a magnetic field that are perpendicular to each other and to the propagation of the wave. Usually, light is unpolarized with electric fields of random orientations and phases. Polarization of light restricts its electric field to a well-defined shape and path. Linearly polarized light consists of two orthogonal waves that are in phase, tracing out a straight line by its electric field vector on a fixed plane as it propagates (Figure 6a). When these two waves are equal in amplitude but are out of phase by 90° , they constitute a circularly polarized light (Figure 6b). Ellipsometry uses elliptically polarized light by combining two orthogonal waves of random amplitude and phase difference ($\neq 0^\circ$ or 90° , Figure 6c).³⁹

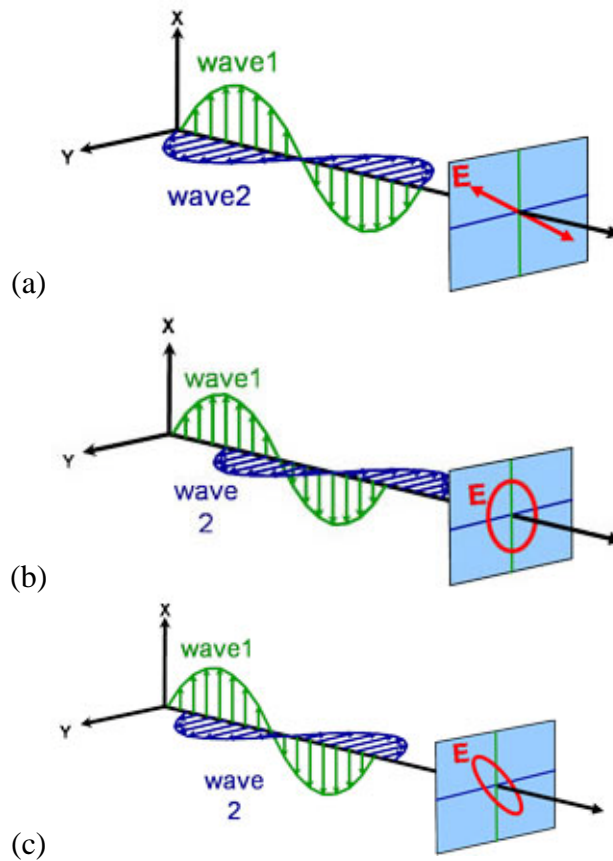


Figure 6. Examples of light polarization: (a) linearly, (b) circularly, and (c) elliptically polarized light.⁴⁰

When a light beam reaches an interface between two materials of different optical densities, reflection and/or refraction occur. The law of reflection (Figure 7a) states that the angle of incidence is equal to the angle of reflection, i.e.,

$$\theta_i = \theta_r. (1)$$

Refraction is governed by the Snell's law (Figure 7b), i.e.,

$$n_1 \sin \theta_1 = n_2 \sin \theta_2, (2)$$

where n_1 and n_2 denote the refractive indices of the materials, which increase as the optical densities increase. θ_1 and θ_2 denote the incident and refracted angles

respectively. Total internal reflection occurs when light travels from a material into an optically less dense material at an incident angle greater than the critical angle. In this condition, all the light is reflected and refraction does not occur.

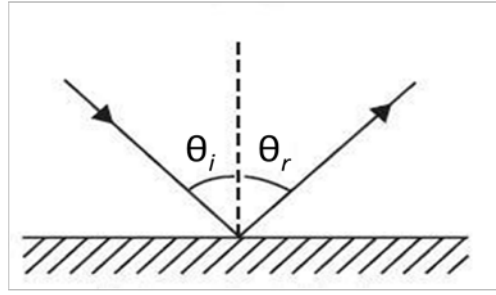


Figure 7(a). *Law of reflection.*

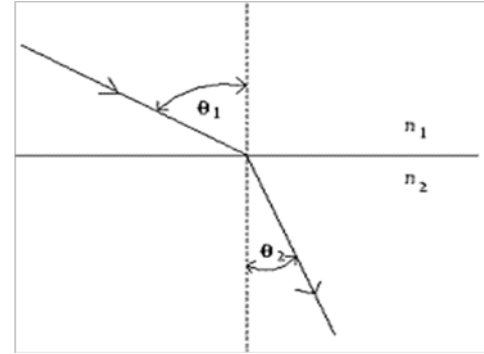


Figure 7(b). *Snell's law.*

When an elliptically polarized light beam reaches multiple interfaces (Figure 8), both reflection and refraction occur. The wave that is parallel to the plane of incidence is referred as the p wave and the one that is perpendicular to the plane of incidence is referred as the s wave. There are four physical parameters crucial to the operation of an ellipsometer. First, the Fresnel reflection coefficient, r , describes the ratio of the amplitude of the reflected wave to that of the incident wave in the p and s directions,⁴¹ i.e.,

$$r_{12}^p = \frac{N_2 \cos \theta_1 - N_1 \cos \theta_2}{N_2 \cos \theta_1 + N_1 \cos \theta_2} \text{ and } r_{12}^s = \frac{N_1 \cos \theta_1 - N_2 \cos \theta_2}{N_1 \cos \theta_1 + N_2 \cos \theta_2}. \quad (3)$$

N_1 and N_2 denote the complex refractive indices of the materials, taking into consideration the extinction coefficients. r_{23}^p and r_{23}^s are defined in the same manner.⁴¹

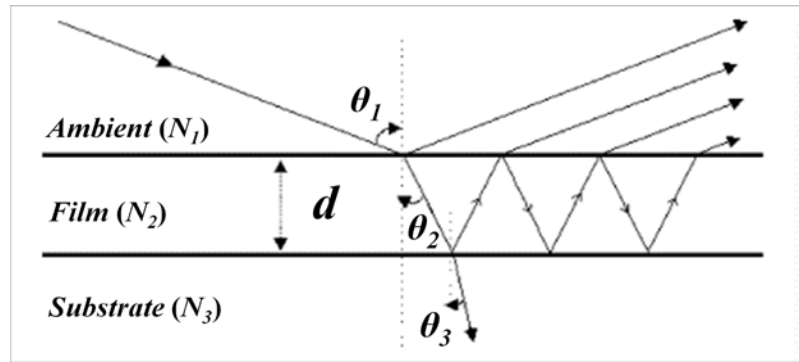


Figure 8. Reflections and refractions at multiple interfaces.

The reflection coefficient r is related to the total reflection coefficient, R , by

$$R^p = \frac{r_{12}^p + r_{23}^p e^{-i2\beta}}{1 + r_{12}^p r_{23}^p e^{-i2\beta}} \text{ and } R^s = \frac{r_{12}^s + r_{23}^s e^{-i2\beta}}{1 + r_{12}^s r_{23}^s e^{-i2\beta}}. \quad (4)$$

where β , the film phase thickness, is given by

$$\beta = 2\pi \left(\frac{d}{\lambda} \right) N_2 \cos \theta_2, \quad (5)$$

and d is the thickness of the interested surface layer and λ is the wavelength.⁴¹

Thirdly, reflectance \bar{R} is defined as the ratio of the reflected intensity to the incident intensity,⁴¹ i.e.,

$$\bar{R}^p = |R^p|^2 \text{ and } \bar{R}^s = |R^s|^2. \quad (6)$$

An ellipsometer directly measures two physical quantities, Δ and Ψ .⁴¹ The parameter Δ is the change in phase difference between p - and s -polarized light upon reflection and $\tan \Psi$ is the corresponding amplitude ratio upon reflection. Δ and $\tan \Psi$ are related to the previous quantities (r , R , β , and \bar{R}) through the fundamental equation,

$$\tan \Psi e^{i\Delta} = \frac{\bar{R}^p}{\bar{R}^s}. \quad (7)$$

When the refractive index of the surface layer, N_2 , is known, the thickness of the surface layer, d , can be calculated by a software program.

Instrumentation & data analysis. A basic ellipsometer consists of the following components: (1) a monochromatic light source, (2) polarizers to elliptically polarize the light, (3) a sample stage, (4) an analyzer to determine the state of polarization of the reflected light, and (5) a detector to convert light to electronic signals (Figure 9). The output state of polarization is compared to the input state to yield the thickness or refractive index of the surface layer.

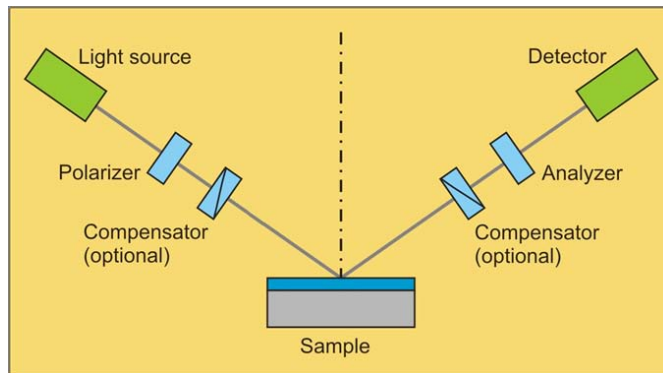


Figure 9. *Ellipsometer components and operation schematic.*⁴²

The ellipsometer used in this study has a He-Ne laser light source with a wavelength of 632.8 nm and a 70° angle of incidence (from the surface normal). Thickness calculations were based on the following parameters: air, $N_1 = 1$; silicon oxide and silane-derived layers, $N_2 = 1.46$; silicon substrate, $N_3 = 3.85$ and $k_3 = -0.02$. The extinction coefficient, k_3 , indicates the amount of absorption loss when light propagates through the silicon substrate. Measurement error is within 1

Å as specified by the manufacturer. The reported thicknesses were averages of four measurements made on different areas of each sample surface.

3.2 Contact Angle Goniometry

General. Contact angle goniometry measures the wettability of a surface, which is its ability to maintain contact with a liquid. It is largely affected by the outermost few Å of the material. This technique measures energetics, physical roughness, and chemical heterogeneities of a surface. Contact angle theories have been introduced in physical chemistry over the last couple of centuries and their applications in surface characterization are usually for qualitative purposes.

Theory. A free liquid drop takes the shape that minimizes the free energy of the system when it rests on a solid surface (Figure 10). The surface free energy is the amount of work required to increase the surface area of a substance by a unit area. A change in the shape of the liquid drop is governed by a change in the free energy of the system, i.e. the Gibbs free energy, and it is demonstrated by the following equation:

$$dG = \gamma^{SL} dA_{SL} + \gamma^{SV} dA_{SV} + \gamma^{LV} dA_{LV}, \quad (8)$$

where γ denotes the surface free energy of the specific interface and it is also referred as the surface tension. dA denotes the change in the surface area of the corresponding interface and by geometry, it fulfills that $dA_{SV} = -dA_{SL}$ and $dA_{LV} = \cos \theta_C dA_{SL}$. Hence, Equation 8 becomes

$$dG = (\gamma^{SL} - \gamma^{SV} + \gamma^{LV} \cos \theta_C) dA_{SL}. \quad (9)$$

At equilibrium where $dG = 0$, γ^{SL} , γ^{SV} and γ^{LV} are related by the Young's equation,⁴³

$$\gamma^{LV} \cos \theta_C = \gamma^{SV} - \gamma^{SL}. \quad (10)$$

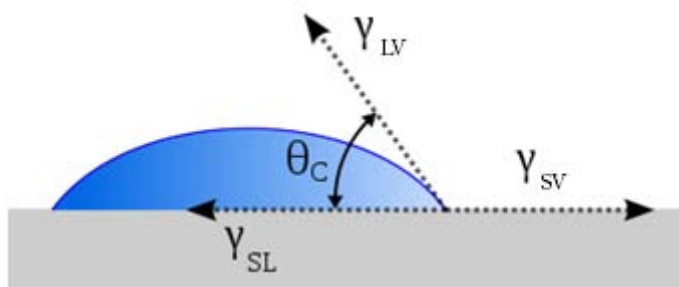


Figure 10. *Static contact angle.*⁴⁴

The Young's equation suggests that the angle θ_C is the outcome of the interactions between the three phases. It is termed static, equilibrium, or intrinsic contact angle and its utilization is based on a few important assumptions. First, the solid surface is smooth and chemically homogenous. Secondly, the solid surface maintains its shape and is not penetrated by the liquid. Thirdly, the functional groups on the solid surface do not react with the liquid. These conditions are rarely met in practical situations. As a result, dynamic contact angles are measured to overcome these limitations. The advancing angle, θ_A , is measured when a liquid drop is added to a solid surface (Figure 11a) and the receding angle, θ_R , is measured when the drop is withdrawn from the surface (Figure 11b). Generally, $\theta_A > \theta_C > \theta_R$ but there are exceptions.



Figure 11. Measurement of dynamic contact angles: (a) an advancing angle and (b) a receding angle.⁴⁵

The difference between θ_A and θ_R is known as the contact angle hysteresis. There are two major categories of hysteresis: thermodynamic hysteresis and kinetic hysteresis. Thermodynamic hysteresis is reproducible over time when the same liquid is applied to the same surface. It is contributed by surface roughness and chemical heterogeneity.⁴⁶ Kinetic hysteresis is time dependent. It is critical when the liquid is able to penetrate the surface with increased contact time and/or when the functional groups on the solid surface are able to reorient after contacting the liquid.⁴⁶ Since silica surfaces used in this study were very stable and did not vary with time, kinetic hysteresis was not significant.

For thermodynamic hysteresis, the Wenzel's equation,⁴⁷

$$\cos \theta_m = r \cos \theta, \quad (11)$$

describes the effect of surface roughness. θ_m is the measured contact angle, θ is the intrinsic contact angle and r , the Wenzel's roughness ratio, is equal to the ratio of the true surface area taking into account of surface roughness to the projected surface area. This relationship suggests that roughening a hydrophilic surface with an intrinsic angle of less than 90° ($\theta < 90^\circ$) decreases the observed angle θ_m .

However, when a hydrophobic surface with an intrinsic angle of greater than 90° is examined, the opposite is observed.

The effect of chemical heterogeneity is described by the Cassie's equation,⁴⁸

$$\cos \theta_m = Q_1 \cos \theta_1 + Q_2 \cos \theta_2. \quad (12)$$

θ_m is the measured contact angle. Q_1 and Q_2 are the fractions of the surface covered by respective regions with contact angles of θ_1 and θ_2 in each phase.

This relationship is established upon the assumption that the surface consists of distinctively defined regions that are large relative to molecular dimensions and therefore the observed angle is a weighted average. In general, this model predicts that the advancing angle is associated with the low-energy regions (hydrophobic) of a heterogeneous surface where the advancing edge of the liquid drop is hindered and the receding angle is associated with the high-energy regions (hydrophilic) where the receding liquid edge is pinned down.

Contact angle provides rich information about both the physical and chemical characteristics of a surface. The complex interactions between the surface and the liquid introduce a variety of important parameters for its measurement. In this study, contact angle measurements were used to assess the extent of hydrolytic degradation of aminosilane-derived layers.

Instrumentation & data analysis. Dynamic contact angles were measured on silicon wafer substrates with Milli-Q water as the probe fluid. Advancing and receding angles were recorded respectively while the probe fluid was released to

and withdrawn from the surface. The reported values were averages of three measurements made on different areas of each sample surface. Within the same batch of samples, the standard deviation of reported values was less than or equal to 2°.

3.3 Atomic Force Microscopy

General. Atomic force microscopy (AFM) investigates and images surface features at nanoscopic resolution. It consists of a sharp tip microfabricated to a soft cantilever. When the tip is in close proximity of a surface, they interact with each other and deflect the cantilever. The deflections of the cantilever correlate with the surface features and the signals are processed to reflect the topography of the surface.

Theory. AFM images are acquired by measuring the deflections of the cantilever due to the interactions between the tip and the surface. The tip-surface interaction encompasses a variety of forces that can be van der Waal's, electrostatic, magnetic and so on. As a result, this technique can be applied to both conducting and insulating materials.

The deflection of the cantilever is governed by Hooke's law,

$$F = -kx, (13)$$

where F is the restoring force exerted by the cantilever that corresponds to the tip-surface force, k is the spring constant that depends on the elasticity of the cantilever material, and x is the displacement of the cantilever from its position of equilibrium. In theory, there are two major modes of operation: constant-height

mode and constant-force mode. In the constant-height mode, the tip is maintained at a fixed height and the tip-surface forces are measured continuously as the tip scans across the surface. The output signals are converted to height information of the surface and plotted against their positions on the sample. This operation mode may cause undesired damages to the sample when the tip touches the surface. In the constant-force mode, the height of the tip is varied to maintain a constant force between the tip and the surface. Again, the output signals are converted to height information of the surface and plotted against their positions. This mode helps to preserve the surface features of a sample.

In practice, the constant-height mode is exemplified by the contact mode AFM. The tip maintains contact with the surface usually through an adsorbed fluid layer on the sample surface. The tip-surface interaction is usually dominated by short-range interatomic forces, which are measured by measuring static cantilever deflections.⁴⁹

The constant-force mode is represented by the tapping mode AFM, which was adopted in this study. The tip-surface interaction is dominated by long-range forces, such as van der Waal's attraction. The tip is attached to a cantilever that oscillates at or near its resonance frequency driven by a piezoelectric element. A change in the tip-surface interaction is detected by changes in the frequency and amplitude of the cantilever. For instance, if the tip is attracted to the surface, the cantilever will oscillate at a lowered frequency and amplitude. In principle, this operation mode is sensitive to single electrons.⁵⁰

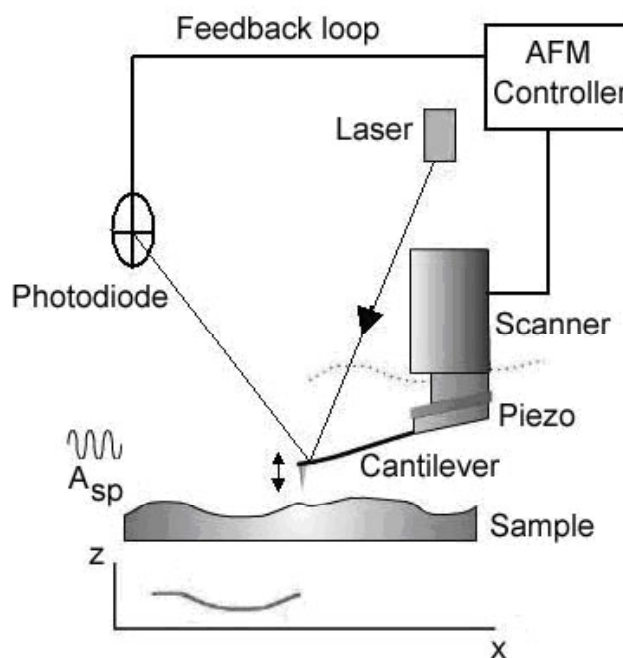


Figure 12. Atomic force microscope components and operation schematic.⁵¹

Instrumentation & data analysis. Tapping mode AFM operates by scanning a tip across a sample surface (Figure 12). The tip with ~ 10 nm of curvature is microfabricated to a cantilever. It gently taps the sample, touching the surface at the bottom of its swing.⁵¹ A feedback loop with a piezoelectric element, which converts electrical energy to mechanical motions, drives the cantilever to oscillate at a constant resonance frequency with an amplitude between 20 nm and 100 nm.⁵¹ Changes in the oscillation of the cantilever are recorded by a photodiode that detects the deflections of a laser beam, focused on the tip at its static position. Larger deflections of the laser beam correspond to higher and lower surface features.

AFM images were acquired and analyzed with the Nanoscope software program. Three-dimensional topography, two-dimensional height profile, and root-mean-square roughness of an image can be determined.

3.4 X-ray Photoelectron Spectroscopy

General. X-ray photoelectron spectroscopy (XPS) detects the relative amounts of elements on a sample surface. It operates based on the photoelectric effect by exciting core electrons on a sample surface and recording both the number and energy of the ejected electrons. Since the energy of the ejected electrons is specific to an element, the identity of the element can therefore be determined. This technique detects all elements except hydrogen and helium.

Theory. When a sample is irradiated with an energetic electromagnetic wave with certain frequency, ν , some core electrons capture the energy and escape from the material. The kinetic energy of the electrons, $K.E.$, is given by,

$$K.E. = h\nu - B.E. - \phi, (14)$$

where h is the Planck's constant, $B.E.$ denotes the binding energy of the electrons, and ϕ denotes the work function of the spectrometer, which is the minimum energy required to remove an electron from a solid to a point immediately outside the solid surface. The binding energy of core electrons in a specific element is known and it is usually in the range of 0 to 1100 eV depending on the electronic structure of the atom. Each element has a unique set of core electrons and their energy states are characteristic of that element.⁵² As a result, the number of ejected electrons is recorded as a function of their binding energy in order to

identify the element and its abundance. This technique is sensitive to the outermost few nanometers of a sample since only the electrons near the surface can overcome inelastic collisions with neighboring atoms to reach the detector.

XPS can also be used for detecting elements at different depths of a sample (Figure 13). This is particularly relevant to this study since the samples were surface-modified and did not have uniform chemical compositions at all depths. This function is achieved by varying the take-off angle between the sample surface and the detector. When the take-off angle is increased, a larger number of electrons are able to escape from the bulk by traveling a shortened distance within the sample, and thus the sample is examined at a greater depth.⁵³

The number of detected electrons, N , is related to the depth via

$$\frac{N}{N_o} = e^{-\frac{t}{\lambda \sin \theta}} \quad (15)$$

where N_o is the number of electrons produced at depth, t , λ is the mean free path of the electron, and θ is the take-off angle.

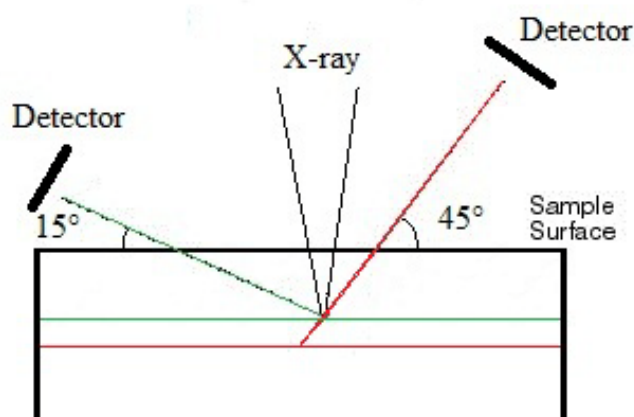


Figure 13. X-ray photoelectron spectroscopy at two take-off angles: 15° and 45°.

Instrumentation & data analysis. A basic X-ray photoelectron spectrometer consists of the following components: (1) an X-ray tube with a magnesium or aluminum anode to produce a monochromatic laser beam, (2) a vacuum chamber to enclose the X-ray and the sample, (3) a neutralizer such as an electron gun to prevent the build-up of surface charges, (4) an electron multiplier to detect the ejected electrons and amplify the signals, (5) an analyzer to record and process the signals (Figure 14).

In this study, an X-ray photoelectron spectrometer equipped with an aluminum anode-laser source was used for detecting C, O, Si, and N contents at two take-off angles, 15° and 45° . The number of scans for each element was adjusted to optimize the signal-to-noise ratio.

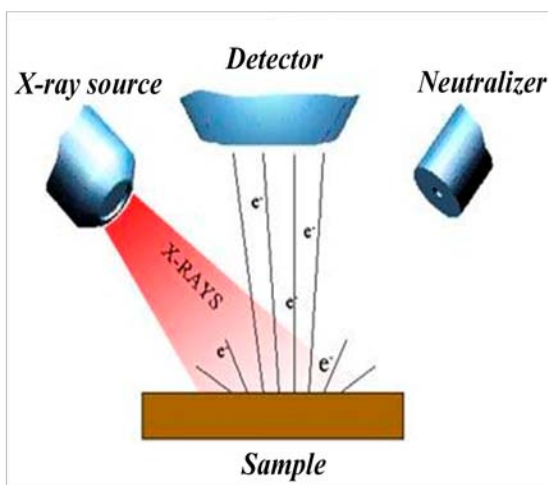


Figure 14. X-ray photoelectron spectrometer components and operation schematic.⁵⁴

4. RESULTS AND DISCUSSION

4.1 Solution-phase Silanization

Overview. Solution-phase silanization was carried out using silane coupling agents from all three groups in anhydrous toluene at 70 °C. The pre-determined conditions were observed to be the most ideal for preparing reproducible and relatively thick aminosilane-derived layers.²³ The hydrolytic stability of aminosilane-derived layers was analyzed as a function of time by submerging freshly silanized samples in Milli-Q water at 40 °C for different amounts of time up to 48 h. Thickness information, contact angle data, and AFM images were acquired before and after hydrolysis and analyzed to assess the hydrolytic stability of respective samples.

Based on their molecular structures, Group I reagents (APTES and APTMS) have a chain length of ~5 Å, Group II reagents (AEAPTES and AEAPTMS) have a chain length of ~8 Å, and Group III reagents (AHAMTES) have a chain length of ~10 Å. As a result, the thicknesses of the corresponding monolayers consisting of closely packed aminosilane molecules should increase in the order of Group I < Group II < Group III. Through experiments, five major factors were identified to have critical impact on the morphology and hydrolytic stability of aminosilane-derived layers: purity of silane coupling agent, ambient humidity, reaction time, nature of silane coupling agent (Group I, II or III), and type of alkoxy group (methoxy group, -OCH₃, or ethoxy group, -OCH₂CH₃). The influence of each factor is elaborated in the following sections.

Silane purity. When 24-h silanization was performed with the Group I reagents, initial thicknesses of ~ 25 Å were obtained with APTES and APTMS as shown in Table 2 and Figure 15. The dynamic water advancing and receding contact angles are much higher than those of a clean silicon wafer, which are $\sim 0^\circ/\sim 0^\circ$ (θ_A/θ_R), as the wafer is extremely hydrophilic with abundant silanol groups on the surface. The increase in dynamic contact angles indicates an increase in hydrophobicity of the surfaces and confirms the fact that aminosilane-derived layers have been attached to the substrates. The thicknesses of the silane layers also suggest that multilayers instead of monolayers have been formed.

After 24-h exposure to water, the multilayers degraded to thicknesses close to those of monolayers. The dynamic contact angles also decreased accordingly. In addition, the reductions in contact angle hysteresis ($\theta_A - \theta_R$) suggest that the physical smoothness and chemical homogeneity of the silane-modified surfaces improved. When the silanized substrates were soaked in water, loosely attached aminosilane molecules were removed from the surfaces, leaving the densely packed monolayers relatively intact, hence improving the physical smoothness of the modified surfaces. The remaining aminosilane molecules on the substrates might also reorient to assume vertical conformations, exposing their primary amine groups to the exterior (Figure 2a). As a result, the hydrolyzed surfaces might have become more hydrophilic and chemically homogeneous, causing dynamic contact angles and contact angle hysteresis to decrease.

Similar trends were observed with silane layers prepared with the Group II reagent AEAPTMS and the Group III reagent AHAMTES. The initial thickness of the AEAPTMS-derived layer was close to those of Group I reagents but its remaining thickness after 24-h hydrolysis in water was higher due to its longer chain. The AHAMTES-derived layer had the most reproducible initial and remaining thicknesses. The decrease in dynamic contact angles was also minimal, indicating a stable silane layer structure.

The striking differences observed between AEAPTES and AEAPTMS were most likely due to their different purities. AEAPTES has the lowest purity, 97.4%, among all the five reagents, giving rise to extremely thick and irreproducible multilayers that degraded extensively during hydrolysis. Although silanization with AEAPTES was carried out under exactly the same conditions, an initial thickness of ~ 280 Å was obtained and its standard deviation (268 Å) among samples prepared in the same batch and different batches was extremely large. After hydrolysis in water, the thickness was reduced drastically to a value that is lower than that of a monolayer, suggesting the exposure of bare silicon wafer substrates.

These observations could arise from the impurities in the silane coupling agent, which may exist in the form of oligomers and polymers of aminosilane molecules introduced during the manufacturing process. These aggregates could be anchored to the substrate surface by very few siloxane bonds and therefore easily removed during hydrolysis. Additionally, the irregular conformations of the

attached aggregates could disrupt the regular arrays of aminosilane molecules, creating structural defects susceptible to water attack. Consequently, these multilayers are not stable in water.

The differences observed between the Group I reagents, APTES and APTMS, could also partly be caused by their different purities. APTMS, with a lower purity (98.5%) than that of APTES (99.7%), produced layers with more variable thicknesses, evident by a larger standard deviation.

Table 2. Thickness and water contact angle (θ_A/θ_R) data of some aminosilane-derived layers before and after 24-h exposure to water.

Group		Purity (%)	Initial		After 24-h hydrolysis	
			Thickness (Å)	Contact angle (deg)	Thickness (Å)	Contact angle (deg)
<i>I</i>	APTES	99.7	23 ± 6	(32 ± 2)/(16 ± 2)	9 ± 4	(24 ± 2)/(14 ± 2)
	APTMS	98.5	26 ± 15	(44 ± 2)/(18 ± 2)	11 ± 4	(27 ± 2)/(15 ± 2)
<i>II</i>	AEAPTES	97.4	282 ± 268	(36 ± 2)/(13 ± 2)	4 ± 2	(31 ± 2)/(14 ± 2)
	AEAPTMS	98.3	24 ± 7	(53 ± 2)/(18 ± 2)	16 ± 7	(42 ± 2)/(14 ± 2)
<i>III</i>	AHAMTES	99.66	21 ± 2	(48 ± 2)/(18 ± 2)	14 ± 4	(49 ± 2)/(18 ± 2)

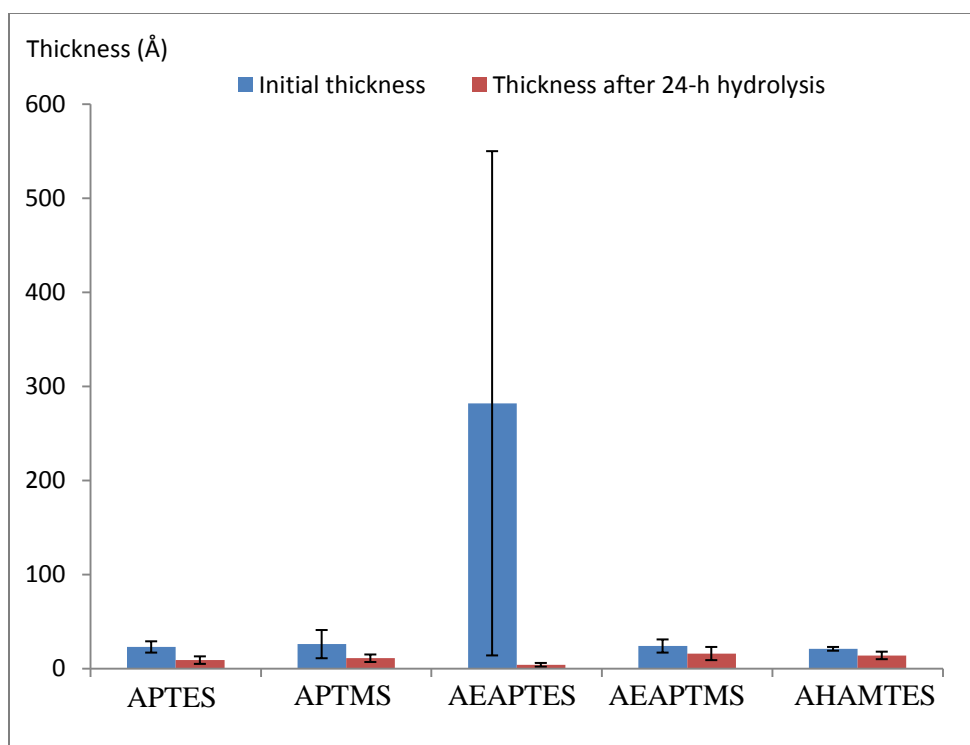


Figure 15. Thickness of aminosilane-derived layers before and after 24-h exposure to water. Solution-phase silanization was carried out in anhydrous toluene at 70 °C for 24 h.

To further confirm the impact of silane purity on the reproducibility of aminosilane-derived layers, silanization reactions were performed in anhydrous toluene at 70 °C for 1 h, 2 h, and 24 h using AEAPTES (97.4% pure), AEAPTMS (98.3% pure), and AHAMTES (99.66% pure). Hydrolysis tests were continued for 48 h to monitor the behaviors of aminosilane molecules in water for an extended period of time. Table 3 illustrates that as the silane purity increased, the standard deviation in the initial thickness of the derived silane layer decreased, indicating an improvement in the reproducibility of the data.

Table 3. Thickness and water contact angle (θ_A/θ_R) data of some aminosilane-derived layers before and after 48-h exposure to water.

	Reaction time (h)	Initial		After 48-h hydrolysis	
		Thickness (Å)	Contact angle (deg)	Thickness (Å)	Contact angle (deg)
AEAPTES (97.4%)	1	94 ± 35	(46 ± 2)/(15 ± 2)	14 ± 1	(34 ± 2)/(14 ± 2)
	2	81 ± 54	(42 ± 2)/(16 ± 2)	4 ± 4	(33 ± 2)/(17 ± 2)
	24	282 ± 268	(36 ± 2)/(13 ± 2)	5 ± 2	(33 ± 2)/(15 ± 2)
AEAPTMS (98.3%)	1	14 ± 4	(52 ± 2)/(18 ± 2)	7 ± 2	(41 ± 2)/(15 ± 2)
	2	14 ± 1	(53 ± 2)/(18 ± 2)	6 ± 2	(38 ± 2)/(13 ± 2)
	24	24 ± 7	(53 ± 2)/(18 ± 2)	17 ± 6	(42 ± 2)/(14 ± 2)
AHAMTES (99.66%)	1	7 ± 3	(47 ± 2)/(22 ± 2)	5 ± 1	(44 ± 2)/(22 ± 2)
	2	13 ± 1	(45 ± 2)/(17 ± 2)	10 ± 2	(43 ± 2)/(20 ± 2)
	24	21 ± 2	(48 ± 2)/(18 ± 2)	12 ± 1	(46 ± 2)/(20 ± 2)

Moreover, an interesting trend was observed with AEAPTES. When the reaction time was increased, the initial thickness of the silane layer increased but its remaining thickness after 48-h hydrolysis decreased. This implies that the thicker layers of AEAPTES probably contained larger amounts of aggregates that reduced the regularity and hence the hydrolytic stability of the derived silane layers. AFM images in Figure 16 confirm this rationale by showing that samples prepared at longer reaction times have more and bigger bright features, which correspond to a larger number of bigger silane aggregates. After hydrolysis, some of the bright features remained on the 1-h silanized sample but disappeared completely on the 24-h silanized sample.

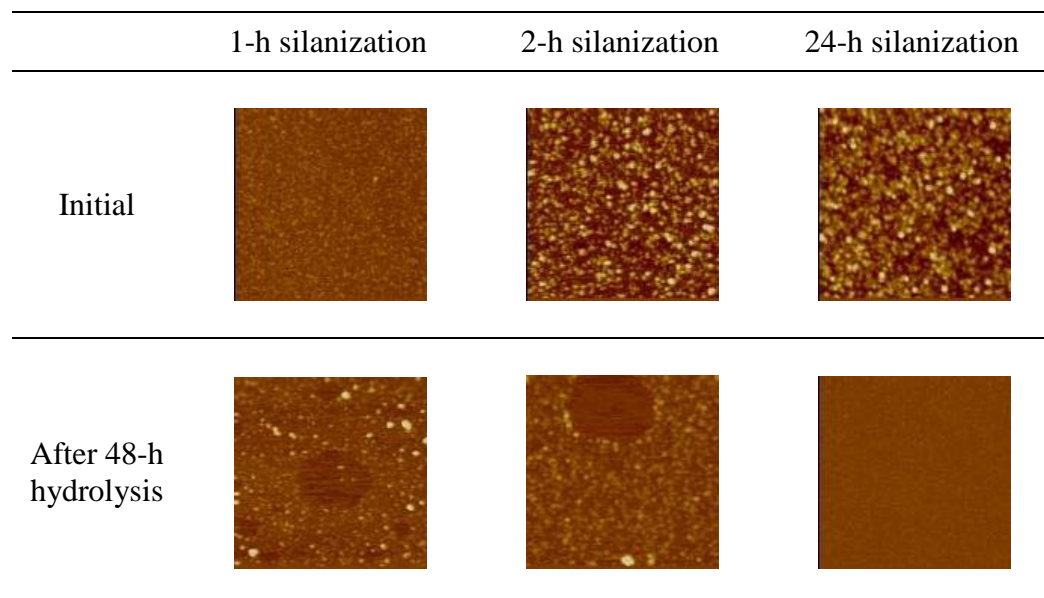


Figure 16. AFM images ($1\ \mu\text{m}\times 1\ \mu\text{m}$, height scale at 20 nm) of AEAPTES-derived layers.

In summary, the purity of a silane coupling agent has a significant impact on the thickness, reproducibility, hydrolytic stability, and morphology of the aminosilane-derived layers. When the silane coupling agents are used as received from their manufacturers without purification, they contain variable amounts of impurities that may be in the form of oligomers and polymers of the aminosilane molecules. They may also form during storage while water diffuses into the reagents, inducing polymerization/aggregation of monomeric aminosilane molecules. These aggregates can be attached to a substrate surface by very few siloxane bonds, giving rise to irregular silane structures. Water therefore can easily penetrate irregularly structured multilayers, cleaves the few siloxane bonds, and removes aggregates from the surface. In order to enhance the hydrolytic stability and reproducibility of aminosilane-derived layers, silane coupling agents

therefore must be purified prior to solution-phase silanization, for instance, by distillation. In the subsequent discussion of other factors, AEAPTES is not included due to the overpowering effect of its low purity.

Ambient humidity. In addition to silane purity, ambient humidity also affects the thickness of aminosilane-derived layers. Illustrated in Figure 17, thicker silane layers were obtained at higher ambient humidity while maintaining the same reaction conditions. More water molecules are present in the reaction system under higher humidity, promoting siloxane bond formation. However, excess water results in the aggregation of aminosilane molecules and hence irregularities in silane layer structures. This drastically decreases the reproducibility of the experiments. As a result, in order to generate reproducible silane layers, only a trace amount of water is required in the reaction medium and the reaction system should be kept as dry as possible.

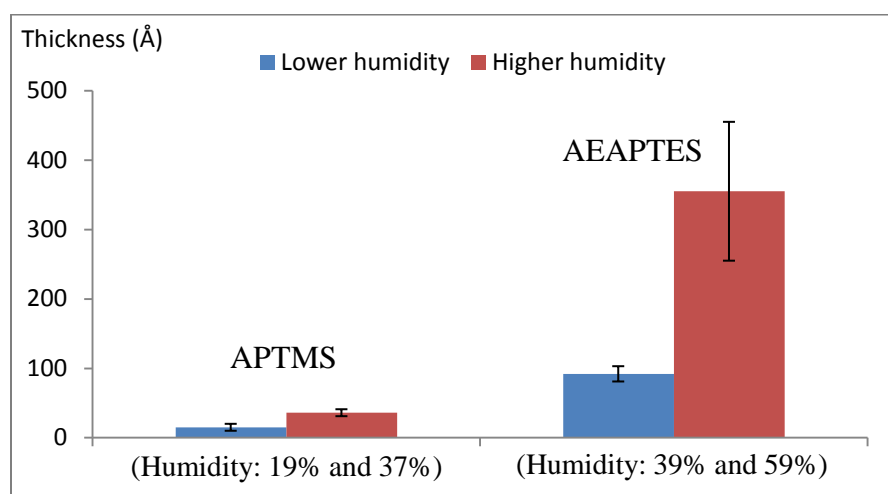


Figure 17. Thickness of APTMS- and AEAPTES-derived layers. Solution-phase silanization was carried out in anhydrous toluene at 70 °C for 24 h under different ambient humidity.

Reaction time. It was reported that the thickness of APTES-derived layer increased as the reaction time was increased.²⁸ The same trend was observed with the Group II reagent AEAPTMS and the Group III reagent AHAMTES when the reaction time was increased from 1 h to 24 h as shown in Figure 18.

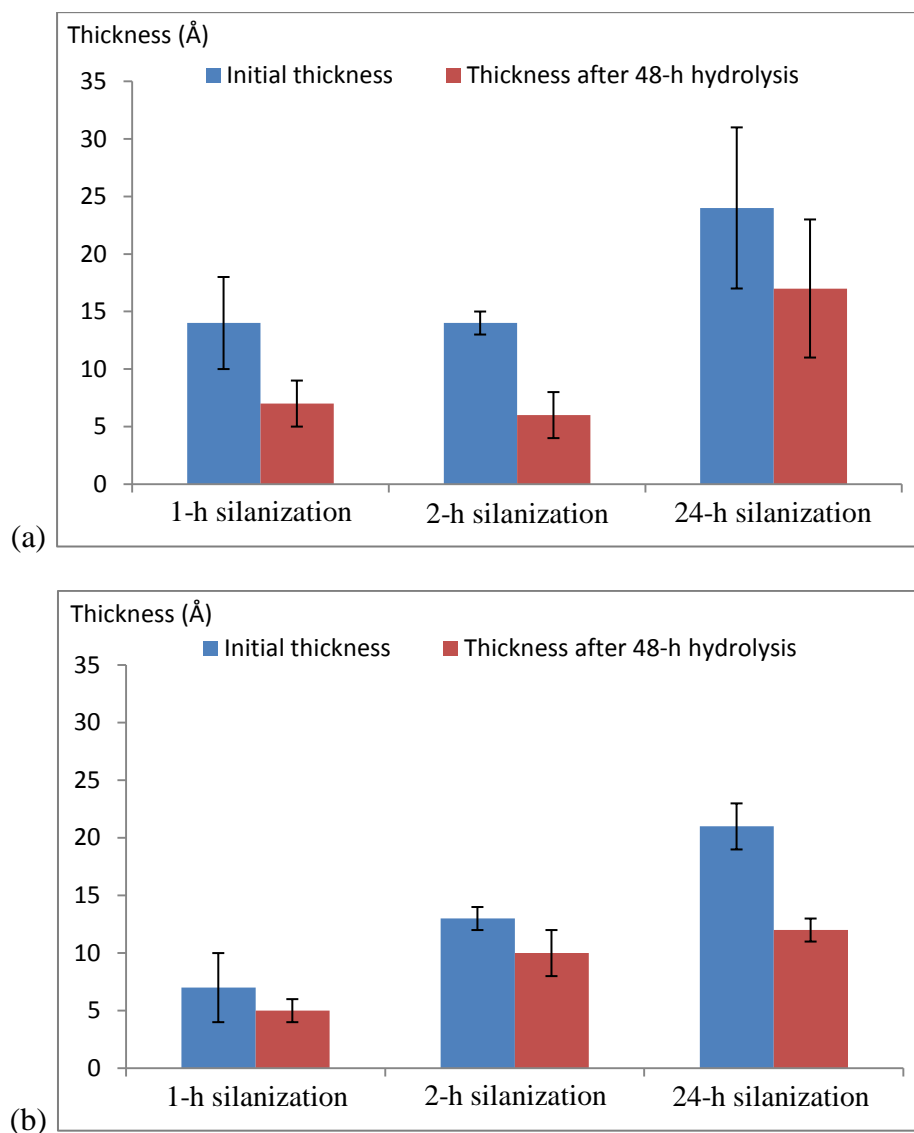


Figure 18. Thickness of aminosilane-derived layers against reaction time: (a) AEAPTMS and (b) AHAMTES. Solution-phase silanization was carried out in anhydrous toluene at 70 °C for 1 h, 2 h, and 24 h, respectively.

As the reaction progresses, more aminosilane molecules are allowed to deposit on the substrate surface. Shown in Figure 18, the remaining thicknesses after soaking in water scale with the initial thicknesses of the silane layers, suggesting that hydrolytic stability could be enhanced by increasing reaction time. However, it is speculated that the multilayers would eventually degrade to monolayers given sufficient hydrolysis time.

Nevertheless, extending reaction time does not necessarily improve the surface morphology of the silane layers. Surface features observed on AFM images of AHAMTES-derived layers (Figure 19) were similar in size and shape for samples prepared at different reaction times. The mean roughness of the surface determined by the Nanoscope software program was also independent of reaction time.

In general, the reaction time for solution-phase silanization can be adjusted accordingly for acquiring the desired thickness of silane layers because their remaining thickness after exposure to water scales with their initial thickness. Silane layers also tend to have comparable surface morphologies that are independent of their thicknesses within 24-h reaction time.

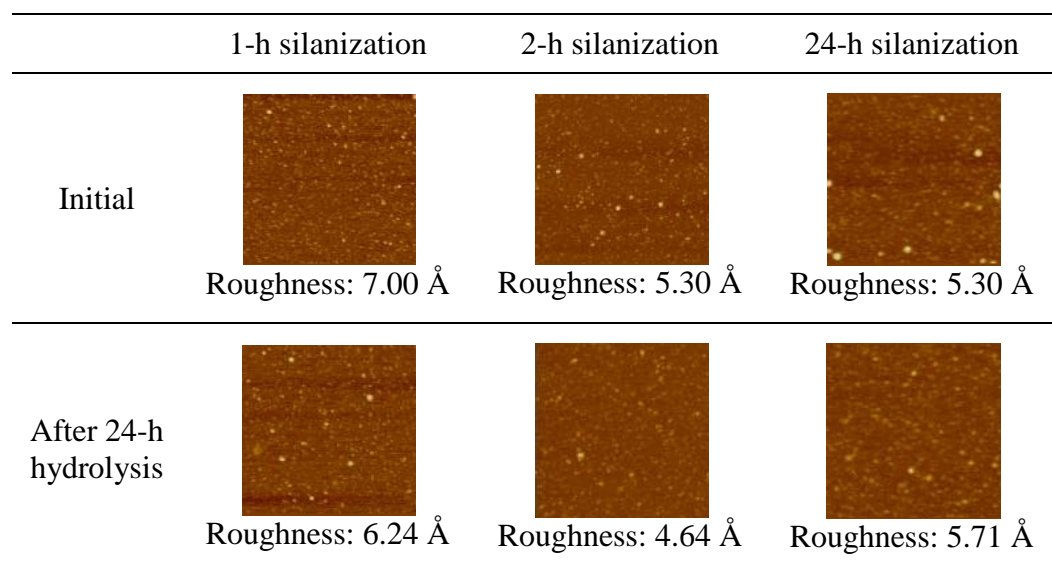


Figure 19. AFM images ($1\ \mu\text{m}\times 1\ \mu\text{m}$, height scale at 20 nm) of AHAMTES-derived layers.

Nature of silane coupling agent. The performance of a silane coupling agent was evaluated based on the thickness, reproducibility, hydrolytic stability, and surface morphology of its silane layers. APTES, the most commonly used silane coupling agent for functionalizing silicon wafers, was used as the standard for comparison. Again, AEAPTES is excluded due to its low purity.

The effect of silane structure on silanization. As shown in Figure 20, the initial thicknesses of aminosilane-derived layers obtained by 24-h silanization were all $\sim 25\ \text{\AA}$. The thickness of silane layers thus appears to be not affected by the structure of the silane coupling agent. All the aminosilanes examined are capable of inter-molecular catalysis in solution, which seems sufficient to produce silane layers of comparable thicknesses.

However, the standard deviation in the thickness of the silane layers increased steadily from the Group III, the Group II, to the Group I reagents.

Variability in the thickness of silane layers could be attributed to the impact of silane purity and the intra-molecularly catalyzed silanization in the Group I and II reagents, which leads to the formation of oligomers of aminosilane molecules in solution and their deposition on substrates. Particularly, the primary amine groups in the Group I reagents have higher tendency to form cyclic intermediates that facilitate the occurrence of intra-molecular catalysis. In addition, tri-methoxy aminosilanes are more sensitive to the ambient humidity than tri-ethoxy aminosilanes and this factor is elaborated further in the subsequent sections. Overall, the reactions with AHAMTES generated the most reproducible silane layers.

The effect of silane structure on hydrolytic stability. Although the initial thicknesses of silane layers were comparable across all three groups of aminosilanes, the remaining thicknesses after 24-h hydrolysis were apparently larger for the Group II and III reagents probably due to their structural features and enhanced hydrolytic stability. Both groups of aminosilanes have longer chains, which hinder the formation of cyclic intermediates, reducing intra-molecularly catalyzed hydrolysis of siloxane bonds.

Kinetic studies for hydrolysis in water were performed with APTES and AHAMTES as shown in Table 4 and Figure 21. The absence of intra-molecular catalysis in AHAMTES is not only manifested by its higher stability but also higher reproducibility of the silane layer thickness after hydrolysis.

The fluctuating thicknesses of silane layers observed during hydrolysis tests could be explained by two reasons. First, the loss of aminosilane molecules from the substrate surface to the surrounding water is governed by a chemical equilibrium. Secondly, the substrate surface might be contaminated.

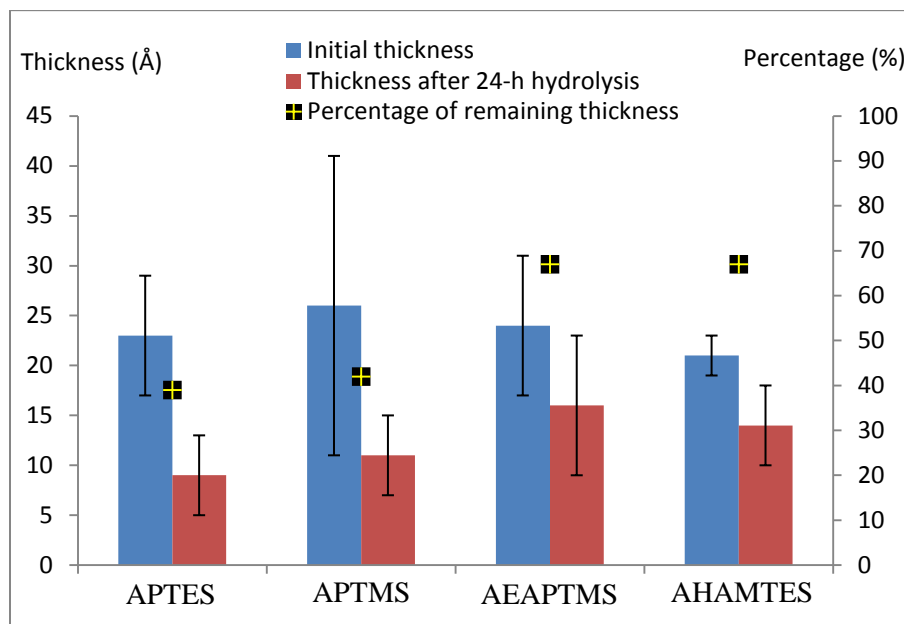


Figure 20. Thickness of aminosilane-derived layers before and after 24-h exposure to water and the percent of remaining thickness. Solution-phase silanization was carried out in anhydrous toluene at 70 °C for 24 h.

Table 4. Thickness of APTES- and AHAMTES-derived layers before and after exposure to water.

Hydrolysis time (h)	Thickness (Å)	
	APTES	AHAMTES
0	22 ± 5	22 ± 1
1	11 ± 1	14 ± 2
3	12 ± 3	15 ± 1
12	9 ± 1	20 ± 4
24	10 ± 3	16 ± 1

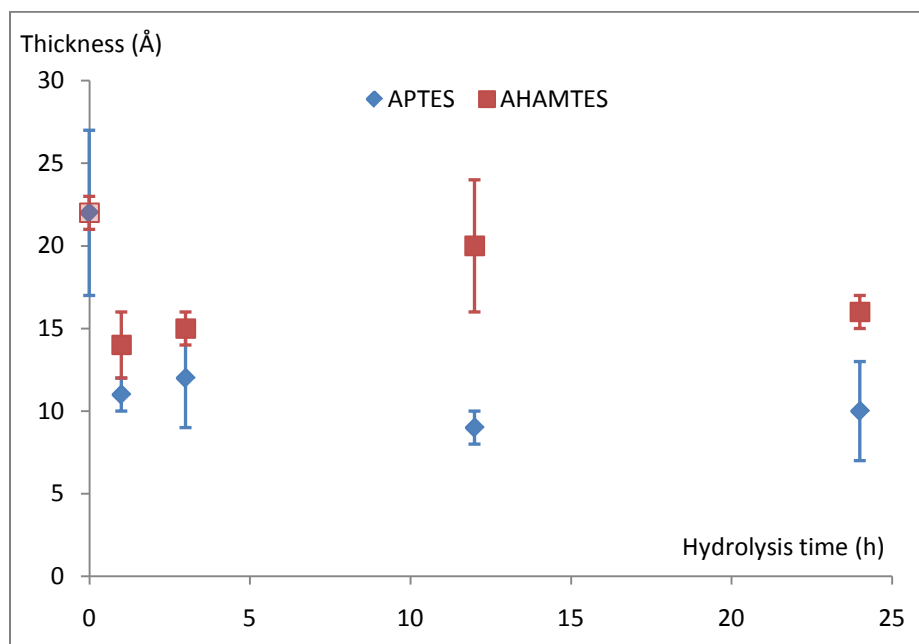


Figure 21. Thickness of APTES- and AHAMTES-derived layers against hydrolysis time (1 h, 3 h, 12 h, and 24 h). Solution-phase silanization was carried out in anhydrous toluene at 70 °C for 24 h.

Number of alkoxy groups. To confirm the superior efficiencies of constructing silane layers with tri-alkoxy aminosilane reagents, solution-phase silanization was carried out with 3-aminopropyltrimethoxysilane (APTMS, 97% pure) under the same reaction conditions. As shown in Table 5 and Figure 22, the initial thicknesses of its silane layers were close to that of a monolayer independent of the reaction time. After 24-h soaking in water, almost all the silane layers degraded. This is most likely due to the presence of a single ethoxy group per molecule that limits the number of anchoring sites on a substrate surface and eliminates the possibility of cross-linking with neighboring molecules.

Additionally, the methyl groups on APTMS prevent the formation of silane

monolayers of high density, and hence the ease of water penetration in between the attached aminosilane molecules renders them hydrolytically unstable. As a result, tri-alkoxy aminosilanes are more efficient functionalizing reagents.

Table 5. Thickness and water contact angle (θ_A/θ_R) data of APDMES-derived layers before and after 24-h exposure to water.

	Reaction time (h)	Initial		After 24-h hydrolysis	
		Thickness (Å)	Contact angle (deg)	Thickness (Å)	Contact angle (deg)
APDMES (97%)	1	5 ± 1	(52 ± 2)/(40 ± 2)	0 ± 1	(21 ± 2)/(17 ± 2)
	2	6 ± 1	(52 ± 2)/(35 ± 2)	1 ± 1	(43 ± 2)/(17 ± 2)
	24	5 ± 1	(52 ± 2)/(40 ± 2)	1 ± 1	(25 ± 2)/(16 ± 2)

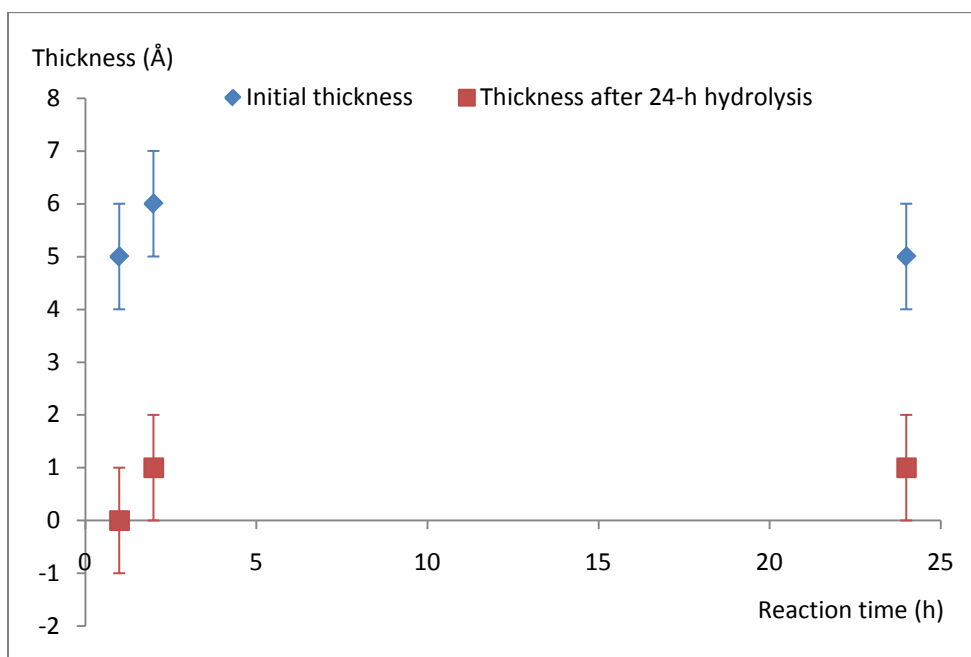


Figure 22. Thickness of APDMES-derived layers before and after 24-h exposure to water against reaction time. Solution-phase silanization was carried out in anhydrous toluene at 70 °C for 1 h, 2 h, and 24 h, respectively.

Type of alkoxy group. In theory, tri-methoxy aminosilanes are more reactive than tri-ethoxy aminosilanes since methoxy is a better leaving group. Our

results corroborate this prediction. Based on the comparison between APTES and APTMS of comparable purities (Table 2), the thickness of APTES-derived layer ($23 \pm 6 \text{ \AA}$) was more reproducible than that of the APTMS-derived layer ($26 \pm 15 \text{ \AA}$). Similar comparisons between the reagents in Group II and III are not available due to the low purity of AEAPTES and the unavailability of methoxy-based Group III reagents.

Faster silanization with tri-methoxy aminosilanes is less controllable and could render the silane layers less regular in structure. At the solid-solution interface, the tri-methoxy aminosilane molecules are deposited on the substrate more rapidly. Before the molecules could orient themselves in favorable conformations, more molecules are deposited on top. Polymerization of tri-methoxy aminosilanes in solution is also expected to occur at faster rates. Consequently, tri-methoxy aminosilane-derived layers are more irregular and less reproducible.

In general, there is a trade-off between rate and reproducibility in silanization reactions. However, since both trimethoxy and triethoxy aminosilane reagents were observed to give rise to silane layers with similar thicknesses in the same amount of reaction time, tri-ethoxy aminosilanes that confer higher reproducibility are more desirable.

Summary. Generally, silane layers produced in solution-phase reactions are typically multilayer in nature with some surface roughness. The reproducibility of solution-phase silanization is highly dependent on the purity of

a silane coupling agent and the ambient humidity. As a result, purification of the silane coupling agent and maintenance of a dry reaction system are essential for generating reproducible silane layers. The hydrolytic stability of aminosilane-derived layers can also be enhanced by extending reaction time, which does not necessarily alter their surface morphologies. Furthermore, two major considerations are involved in choosing a suitable silane coupling agent, which are the nature (methoxy or ethoxy) and the number (mono-, di-, or tri-alkoxy) of the alkoxy group and the molecular structure of the aminosilane molecule (Group I, II, or III). Based on this study, AHAMTES, a Group III reagent with the highest purity of 99.66%, was shown to generate the most reproducible and hydrolytically stable silane layers via solution-phase silanization.

4.2 Vapor-phase Silanization

Overview. The significant dependence of solution-phase silanization on silane purity and ambient humidity led us to vapor-phase silanization. In a closed environment, a silane coupling agent reaches an equilibrium vapor pressure at moderate temperatures. The silane molecules in the vapor phase can react with silanol groups on silicon wafers at the solid-vapor interface. Impurities in the form of aggregates do not readily vaporize due to their higher boiling points and therefore they will not deposit on a substrate surface. The impact of ambient humidity should also be minimal since the reaction system can be kept consistently drier in the absence of a solvent. Developing a reliable protocol for

vapor-phase silanization hence greatly simplifies substrate modification with aminosilane reagents.

Vapor-phase silanization was attempted using silane coupling agents from all three groups. The reaction conditions such as temperature, time, and drying conditions were optimized to maximize the reproducibility and hydrolytic stability of aminosilane-derived layers. The hydrolytic stability was analyzed as a function of time by submerging freshly silanized samples in Milli-Q water at 40 °C for various amounts of time up to 24 h or 48 h. Thickness information, contact angle data, AFM images, and XPS analyses were acquired before and after hydrolysis and analyzed to assess the hydrolytic stability of respective samples.

Initial survey. Initial studies were carried out with the Group II reagents AEAPTES and AEAPTMS to survey the factors that could play critical roles in vapor-phase reactions.

First of all, vapor-phase silanization is found to be indeed independent of silane purity. Shown in Table 6, the AEAPTES of a lower purity (97.4%) generated more uniform and reproducible silane layers than the AEAPTMS of a higher purity (98.3%). As mentioned earlier, the impurities in the silane coupling agent do not vaporize easily and thus do not react with the substrate surface. Therefore, purification of a silane coupling agent is not essential for vapor-phase reactions.

Secondly, the initial thickness of aminosilane-derived layers can be increased by raising the reaction temperature. When the vapor-phase reactions

were performed for 48 h without purging the reaction tubes, the reactions at 90 °C generated thicker silane layers than those at 70 °C, as shown in Table 6. Raising the reaction temperature increases the vapor pressure and the reaction rate, allowing more aminosilane molecules to deposit on the substrate surfaces. After 48-h soaking in water, the remaining thicknesses of AEAPTES-derived layers were close to that of a monolayer, suggesting that the two chosen temperatures were sufficiently high for obtaining stable silane structures.

The third factor is the amount of water in the reaction system. It was observed that without purging, the reproducibility of the initial thickness was lower at the higher reaction temperature, which was improved by purging the reaction tube under N₂ for 4 min (Table 6). However, this led to the formation of thinner multilayers. Reducing the amount of water in the reaction system decreases the chances of vertical polymerization of aminosilane molecules and hence enhances the regularity of aminosilane-derived layers.

Furthermore, the nature of alkoxy group also affects the reproducibility and hydrolytic stability of aminosilane-derived layers. Under all three sets of reaction conditions, the thicknesses of AEAPTMS-derived layers were much less reproducible than those of AEAPTES-derived layers. The lower reproducibility of AEAPTMS could be explained by the higher reactivity of tri-methoxy aminosilanes. Consistent with our observations in the solution-phase silanization, tri-ethoxy aminosilanes gave rise to more reproducible silane layers in the vapor-phase reactions and therefore are the more preferred tri-alkoxy aminosilanes.

Table 6. Thickness of AEAPTES- and AEAPTMS-derived layers before and after 48-h exposure to water.

	Thickness (Å)					
	48 h, 70 °C, no purging under N ₂		48 h, 90 °C, no purging under N ₂		48 h, 90 °C, 4 min- purging under N ₂	
	Initial	After	Initial	After	Initial	After
AEAPTES (97.4%)	14 ± 2	11 ± 1	27 ± 22	9 ± 3	15 ± 4	10 ± 3
AEAPTMS (98.3%)	157 ± 109	4 ± 2	521 ± 366	13 ± 9	34 ± 35	7 ± 1

Fine-tuning reaction conditions – minimizing the impact of ambient humidity. In the initial survey, it was observed that purging reaction tubes under N₂ for 4 min improved the reproducibility of the experiments. To further remove excess water and minimize the impact of ambient humidity, purging time was extended to 30 min. In addition, the seal of the glassware was improved by tightening the joints.

Adjusting reaction time and temperature. In the attempt to enhance the reproducibility of the experiments, 24-h vapor-phase reactions at 70 °C with 30-min purging under N₂ were carried out with the Group I reagents (APTES & APTMS) and Group II reagents (AEAPTES & AEAPTMS). The initial thicknesses of the AEAPTMS- and AEAPTES-derived layers decreased to 19 ± 17 Å and 5 ± 1 Å respectively (Table 7 and Figure 23). Compared to the 48-h reactions at 90 °C with 4-min purging (Table 6), these adjustments improved the reproducibility of the data at the expense of the thickness of the silane layers.

Shown in Table 7 and Figure 23, the initial thickness of the APTMS-derived layer was less reproducible than that of the APTES-derived layer, which again is probably because tri-methoxy aminosilanes have higher reactivity, resulting in more sample variations. Therefore, only tri-ethoxy aminosilanes were focused on in the vapor-phase study.

In addition, it is apparent that the APTES- and AEAPTES-derived layers generated in the extensively purged reaction systems at 70 °C were too thin to be hydrolytically stable. Reaction temperature was therefore set at 90 °C for the subsequent experiments with all tri-ethoxy aminosilanes.

Table 7. *Thickness of the Group I and II aminosilane-derived layers before and after exposure to water.*

		Purity (%)	Thickness (Å)		
			Initial	After 1-h hydrolysis	After 24-h hydrolysis
<i>Group I</i>	APTES	99.7	6 ± 1	2 ± 1	3 ± 1
	APTMS	98.5	13 ± 9	9 ± 7	9 ± 5
<i>Group II</i>	AEAPTES	97.4	5 ± 1	3 ± 1	2 ± 1
	AEAPTMS	98.3	19 ± 17	9 ± 5	4 ± 1

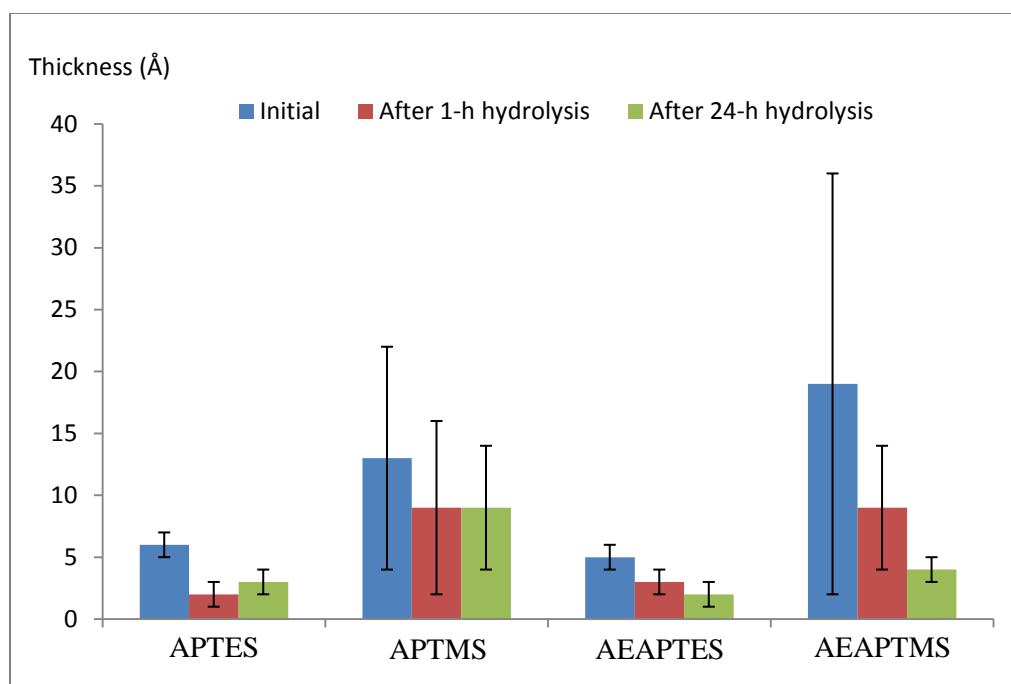


Figure 23. Thickness of aminosilane-derived layers before and after exposure to water. Vapor-phase silanization was carried out at 70 °C for 24 h.

Vapor-phase silanization with AHAMTES. When the 48-h vapor-phase reactions were carried out with the Group III reagent AHAMTES at 90 °C with 30-min purging under N₂, the initial thickness was extremely low as shown in Table 8. Attempts to increase the silane layer thickness were made by eliminating the purging step to retain water in the reaction system and increasing the reaction temperature to 100 °C and 110 °C. Under adjusted conditions, the silane layers were either still too thin or unstable in water.

As mentioned in the introduction section, the amine group in AHMATES is only capable of catalyzing silanization inter-molecularly. The silane molecules are much further apart in the vapor phase than in the solution phase, and hence intermolecular interactions are likely to be absent. Intra-molecular amine-catalysis

thus appears to be important for obtaining silane layers with appreciable thicknesses in vapor-phase silanization at moderate temperatures. AHAMTES is the best choice for solution-phase silanization due to its high purity and molecular structure as discussed earlier, however, it is shown here that AHAMTES or any Group III aminosilane reagent is not suitable for vapor-phase silanization due to the lack of intra-molecular amine-catalysis.

Table 8. *Thickness of AHAMTES-derived layers before and after 48-h exposure to water.*

	Thickness (Å)							
	48 h, 90 °C, purging under N ₂		48 h, 90 °C, no purging		48 h, 100 °C, no purging		48 h, 110 °C, no purging	
	Initial	After	Initial	After	Initial	After	Initial	After
AHAMTES (99.66%)	2 ± 1	1 ± 1	2 ± 1	1 ± 1	23 ± 5	5 ± 1	140 ± 97	8 ± 5

Vapor-phase silanization with APTES and AEAPTES. Based on all the initial studies, we decided to focus on investigating vapor-phase silanization with the Group I reagent APTES and the Group II reagent AEAPTES. The reaction temperature, 90 °C, was found to be sufficiently high for producing aminosilane-derived layers with acceptable thicknesses and homogeneous morphologies (Table 9). The impact of reaction time was analyzed by characterizing the hydrolytic stability and surface morphology of the silane layers prepared by either 24-h or 48-h reactions.

Hydrolytic stability. The hydrolytic stability of aminosilane-derived layers was analyzed by examining their thickness and contact angle after different

durations of soaking in water. For the APTES-derived layers, under purged conditions, increasing the reaction time from 24 h to 48 h did not increase the thickness or the hydrophobicity of the surfaces, indicated by their contact angle measurements (Table 9a). The percent loss of thickness over time (Figure 24) did not differ significantly between the samples prepared under these conditions. However, when the reactions were allowed to take place without purging, the initial thicknesses increased for both sets of conditions. The samples prepared in the unpurged 48-h reactions had the greatest initial thickness, which degraded to a value close to that of a monolayer. The dynamic contact angles were also higher at each time point, indicating the more hydrophobic nature of the surfaces. Additionally, the percent loss of thickness over time was more gradual than the samples prepared in the 24-h unpurged silanization, indicating a slower rate of loss. These observations suggest that increasing the reaction time coupled with a slight increment of the amount of water in the reaction system could enhance the hydrolytic stability of the aminosilane-derived layers by increasing their initial thickness. However, the major drawback of eliminating the purging step is to expose the reaction to fluctuating ambient humidity that decreases the reproducibility of the experiments.

For the AEAPTES-derived layers, increasing the reaction time increased their initial thicknesses under both purged and unpurged conditions. Particularly under the purged conditions, the samples prepared by 48-h silanization exhibited the slowest rate of loss (Figure 24). It is worth noting that these vapor-phase

reactions under purged conditions generated silane layers corresponding to monolayer thickness: ~ 5 Å for APTES and ~ 8 Å for AEAPTES.

In summary, the Group I and II reagents with either a primary or a second amine group at propyl position, which can catalyze silanization intra-molecularly, yield silane layers with appreciable thicknesses on silicon wafers at moderate reaction temperatures in the vapor phase. The thickness and contact angle data suggest that AEAPTES-derived layers are more hydrolytically stable than APTES-derived layers, similar to our findings in the solution-phase silanization; the most stable amine-functionalized surface was prepared by silanization with AEAPTES at 90 °C for 48 h under purged condition. This observation can be explained by the molecular structures of Group II reagents. Their longer chains are less likely to bend toward the silicon atom due to steric hindrance and therefore intra-molecularly catalyzed hydrolysis of siloxane bonds occurs to a much less extent.

Table 9. Thickness and contact angle (θ_A/θ_R) data of aminosilane-derived layers before and after exposure to water: (a) APTES and (b) AEAPTES.

(a) APTES

	Reaction time (h)	Initial		After 1-h hydrolysis		After 3-h hydrolysis		After 24-h hydrolysis	
		T. * (Å)	C.A.* (deg)	T. (Å)	C.A. (deg)	T. (Å)	C.A. (deg)	T. (Å)	C.A. (deg)
Purged	24	5 ± 1	50/23	3 ± 1	40/17	3 ± 1	36/14	3 ± 1	34/15
	48	5 ± 1	51/23	2 ± 1	36/14	2 ± 1	36/16	3 ± 1	37/15
Not purged	24	8 ± 1	56/32	4 ± 1	40/19	3 ± 1	35/19	3 ± 1	31/17
	48	10 ± 2	55/26	6 ± 2	46/21	6 ± 3	42/20	6 ± 3	36/19

(b) AEAPTES

	Reaction time (h)	Initial		After 1-h hydrolysis		After 3-h hydrolysis		After 24-h hydrolysis	
		T. (Å)	C.A. (deg)	T. (Å)	C.A. (deg)	T. (Å)	C.A. (deg)	T. (Å)	C.A. (deg)
Purged	24	6 ± 1	50/24	4 ± 1	42/19	3 ± 1	40/16	3 ± 1	35/17
	48	11 ± 2	51/22	8 ± 1	41/18	8 ± 1	40/17	8 ± 1	38/16
Not purged	24	10 ± 1	52/26	8 ± 2	46/21	7 ± 3	42/21	6 ± 1	36/19
	48	17 ± 1	58/34	12 ± 1	46/21	12 ± 2	45/20	8 ± 1	39/20

**T.* stands for thickness and *C.A.* stands for contact angle. The standard deviation in the contact angle measurement is smaller or equal to 2°.

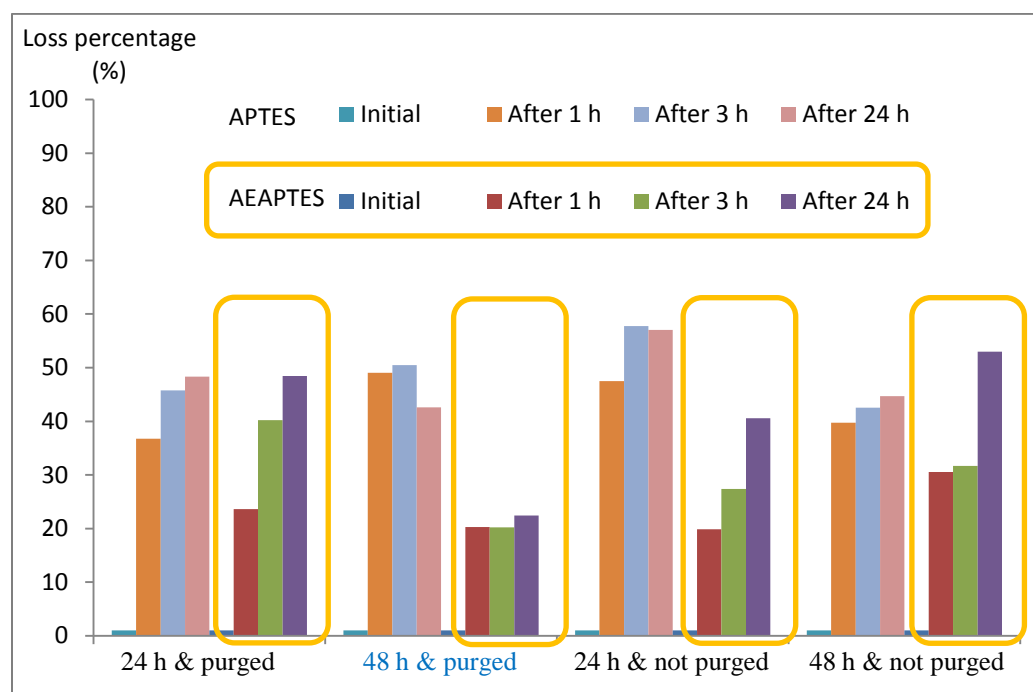


Figure 24. Percent loss of thickness against hydrolysis time: (a) APTES-derived layers and (b) AEAPTES-derived layers. Vapor-phase silanization was carried out at 90 °C for 24 h or 48 h.

Surface morphology. The surface morphologies of the APTES- and AEAPTES-derived layers were examined by AFM. Shown in Figure 25, the surfaces prepared by the 24-h and 48-h reactions under purged conditions were extremely smooth with a mean roughness of ~ 1 Å. After hydrolysis, the surfaces

still appeared smooth and the mean roughness of each sample remained at ~ 1 Å.

This confirms the preparation of monolayers using the vapor-phase approach.

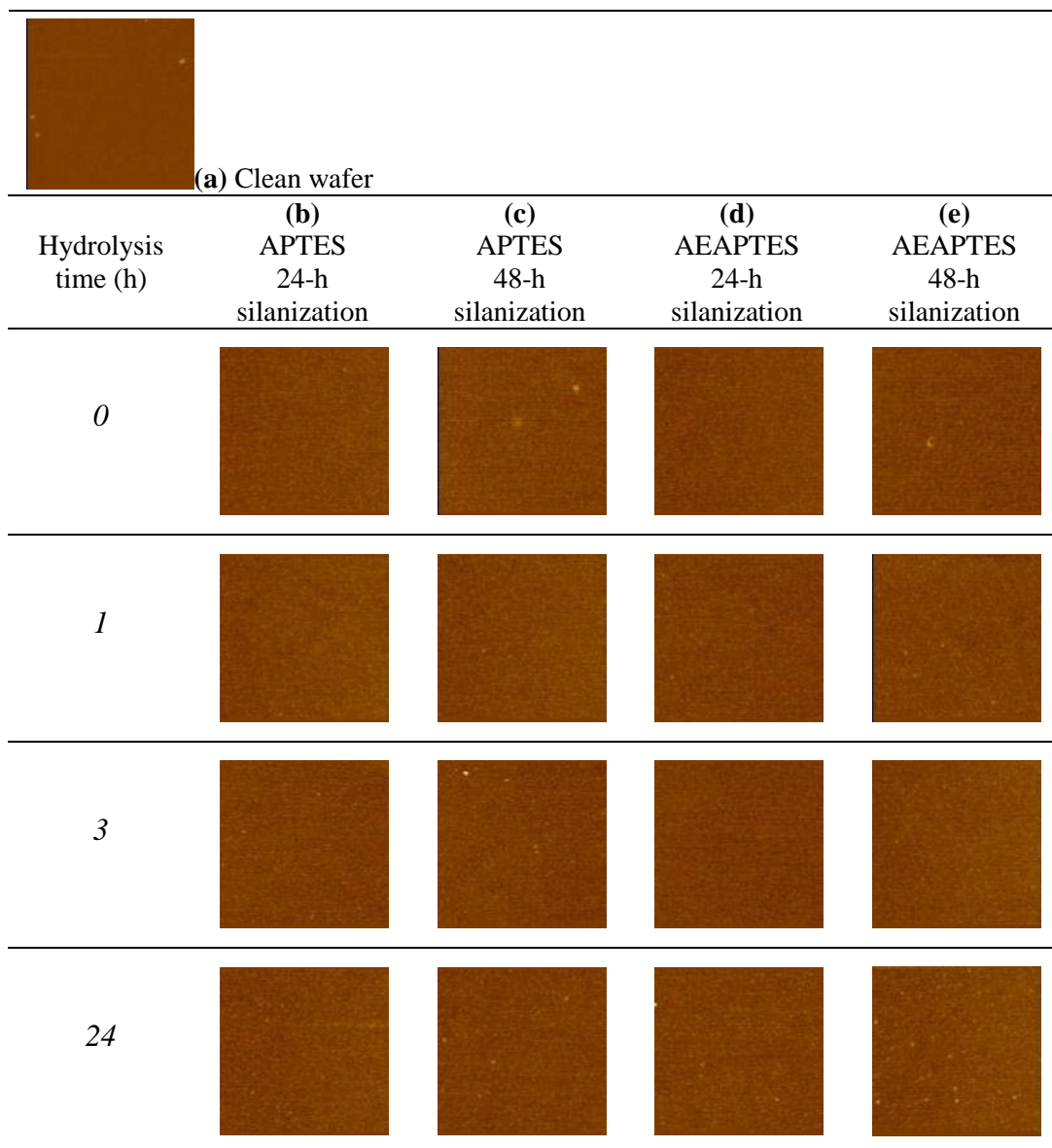
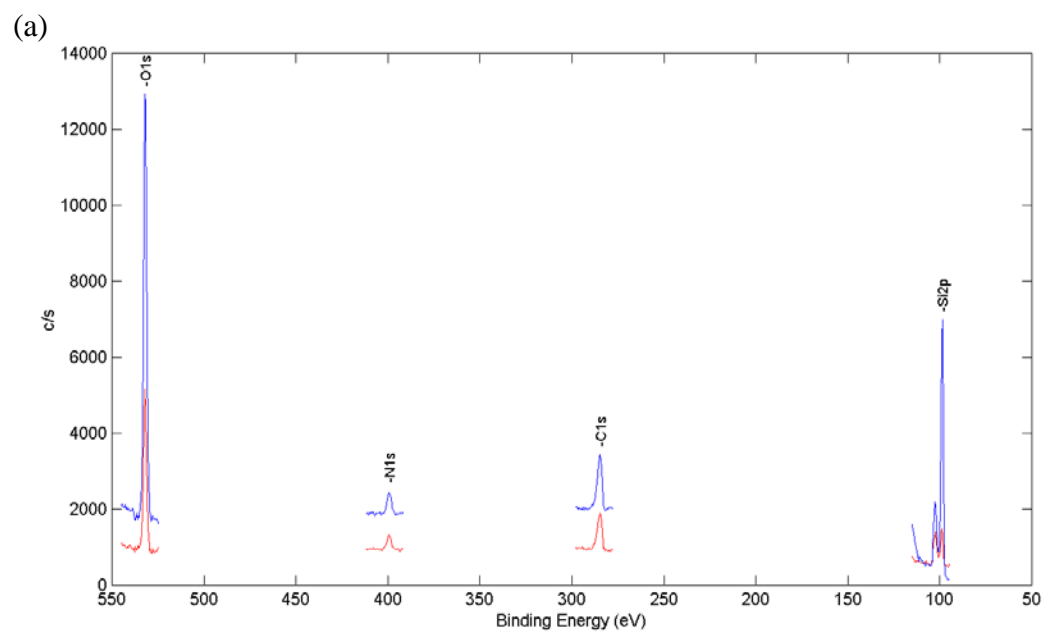


Figure 25. AFM images ($1 \mu\text{m} \times 1 \mu\text{m}$, height scale at 5 nm) of aminosilane-derived layers: (a) clean wafer, (b) APTES-derived layers prepared by 24-h silanization, (c) APTES-derived layers prepared by 48-h silanization, (d) AEAPTES-derived layers prepared by 24-h silanization, and (e) AEAPTES-derived layers prepared by 48-h silanization. The mean roughness for each condition is ~ 1 Å. All the reactions were carried out under purged conditions at 90 °C.

XPS analysis. XPS analysis was carried out at two take-off angles, 15° and 45°, to examine the atomic compositions of the substrate surface, or O, Si, C, and N contents (Figure 26). Oxygen and silicon come mostly from the native silicon oxide layer on the silicon wafers. Carbon and nitrogen are mainly from the attached silane layers. In general, hydrolysis or the loss of the aminosilane layers should result in the exposure of the underlying silicon wafer substrates, which would cause oxygen and silicon contents to increase and carbon and nitrogen contents to decrease. The samples were prepared by 48-h silanization at 90 °C with 30-min purging under N₂. As shown in Table 10, the XPS data obtained at 45° take-off angle consistently show higher silicon signals (from the underlying silicon wafer substrates) and lower oxygen, carbon, and nitrogen signals (from the thin native oxide and silane layers) than those obtained at 15° take-off angle. This is because core electrons ejected at 45° were detected at a greater depth. Since our focus is the outermost silane layers, only the data obtained at 15° will be examined.

As shown in Table 10, for the AEAPTES-derived layers, extending hydrolysis time did not significantly increase the oxygen or the silicon contents, suggesting that the attached silane layers were relatively stable on the substrate surfaces. The carbon and the nitrogen contents decreased slightly after 1-h hydrolysis but then stayed relatively constant, again indicating stable silane structures. These observations were consistent with the thickness and contact angle measurements, which became stable after 1-h hydrolysis (Figure 27b).

The atomic compositions of the APTES-derived layers largely followed a similar pattern (Table 10) but experienced a more rapid loss of its nitrogen contents than the AEAPTES-derived layers, as shown in Figure 28. Combined with the more rapid loss of thickness as shown in Figure 27a, the XPS analysis again suggests that the APTES-derived layers were less hydrolytically stable than the AEAPTES-derived layers. As discussed earlier, molecular structures of the Group II reagents reduce the occurrence of amine catalyzed hydrolysis of siloxane bonds.



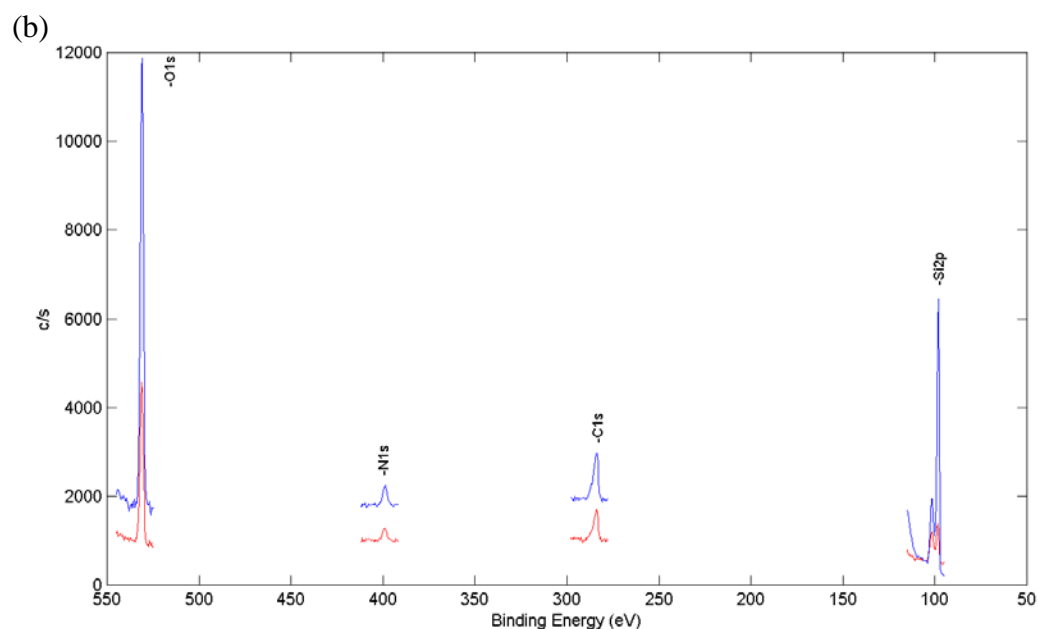


Figure 26. XPS of AEAPTES-derived layers: (a) initial and (b) after 24-h exposure to water. Red features are associated with take-off angle of 15° and blue features are associated with take-off angle of 45° .

Table 10. Atomic compositions of APTES- and AEAPTES-derived layers based on XPS analysis.

		Hydrolysis time (h)		0		1		3		24	
		Take-off angle (deg)		15	45	15	45	15	45	15	45
Relative abundance (%)	APTES	O	42.7	41.0	49.0	42.7	42.8	40.5	46.5	41.9	
		Si	28.4	43.8	33.4	47.9	31.3	45.1	33.4	47.9	
		C	25.3	13.3	14.9	8.3	23.8	13.2	18.1	8.9	
		N	3.8	2.0	2.8	1.2	2.1	1.3	2.1	1.4	
Relative abundance (%)	AEAPTES	O	36.3	37.8	38.6	39.1	39.7	39.8	41.0	39.0	
		Si	25.2	40.9	27.8	41.3	26.0	40.4	25.7	41.2	
		C	31.2	17.2	27.7	15.7	28.3	16.3	27.7	16.1	
		N	7.4	4.1	6.0	3.9	6.1	3.7	5.7	3.7	

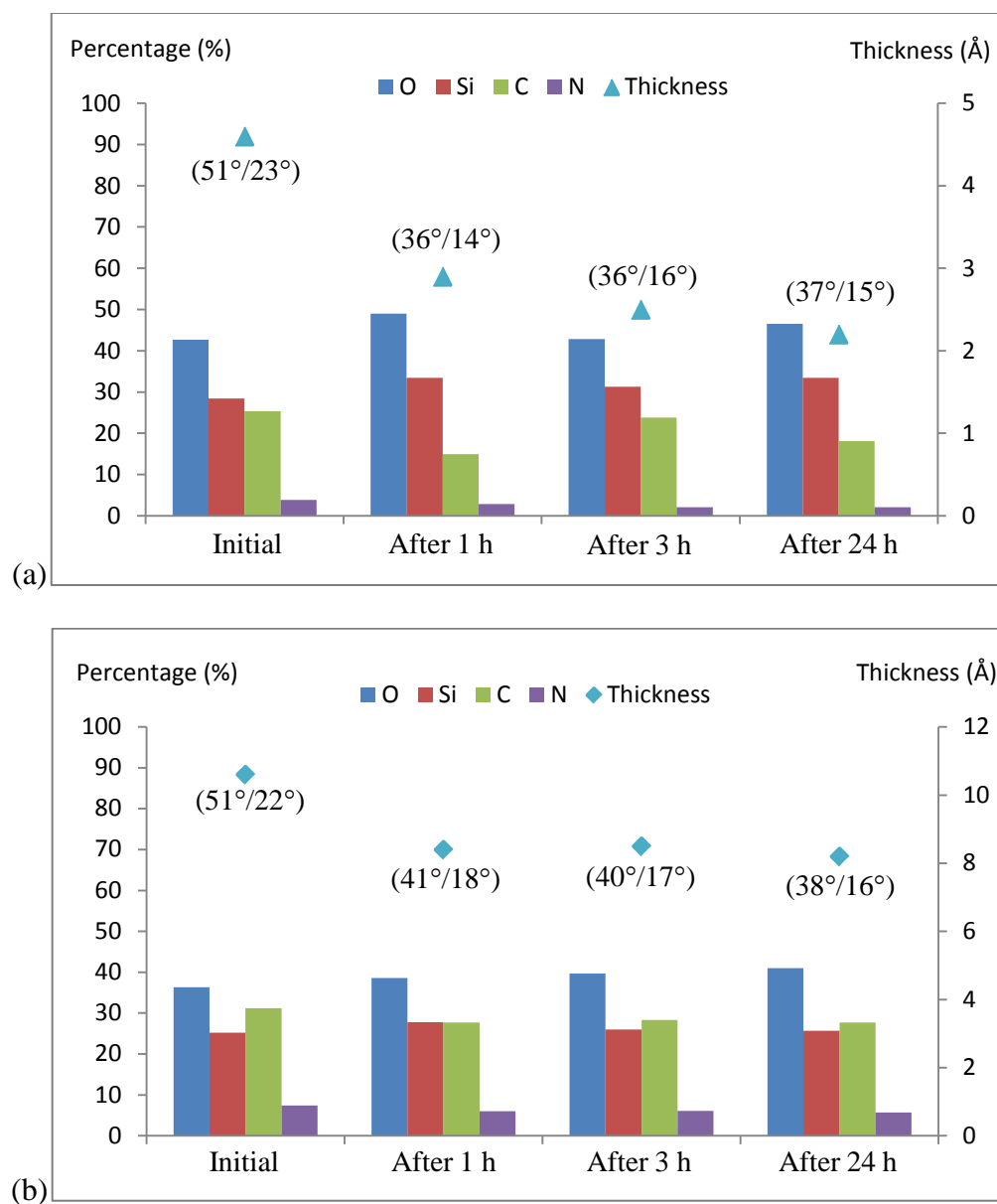


Figure 27. Thicknesses, contact angles and atomic compositions of aminosilane-derived layers: (a) APTES and (b) AEAPTES. Vapor-phase silanization was carried out at 90 °C for 48 h under purged conditions. The standard deviations in the thickness and contact angle are 1 Å and 2°, respectively. The take-off angle for XPS is 15°.

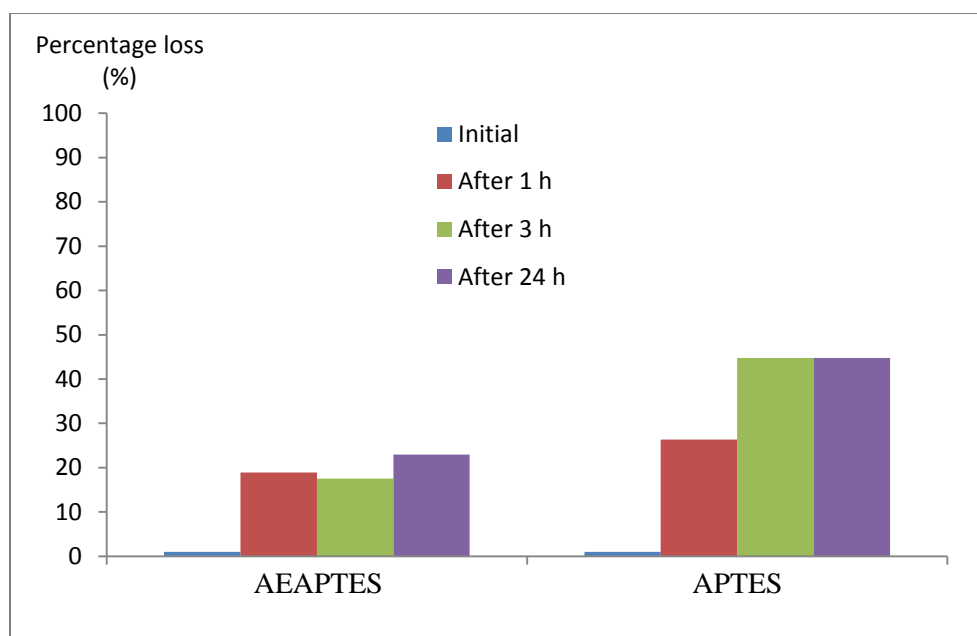


Figure 28. Percent loss of nitrogen content of aminosilane-derived layers based on XPS analysis at the take-off angle of 15°.

Summary. Reproducibility of vapor-phase silanization is independent of silane purity and not affected by ambient humidity under purged conditions. Consistent with solution-phase silanization, reactions with tri-ethoxy aminosilanes are generally more reproducible than those with tri-methoxy aminosilanes since reagents containing ethoxy groups have lower reactivity that makes them more tolerant of fluctuating reaction conditions. In addition, the Group II tri-ethoxy aminosilanes generate the most hydrolytically stable layers. The silane layers derived from the Group I reagents are more susceptible to hydrolysis and Group III reagents are not suitable for vapor-phase reactions due to the lack of intramolecular catalysis by amine functionality.

5. CONCLUSIONS

This was the first comprehensive study in which all commercially available aminosilane reagents were examined and categorized into three groups based on their molecular structures. A total of five representative silanes from these three groups were used to establish necessary structural features and reaction conditions for obtaining hydrolytically stable aminosilane-derived layers on silicon wafer substrates. Categorizing the silane coupling agents into three different groups based on their structural features was shown to be a convenient method to generalize the common characteristics of each group of reagents. In addition, successful attempts were made to optimize reaction conditions for both solution- and vapor-phase silanization to enhance the reproducibility and hydrolytic stability as well as surface morphology of aminosilane-derived layers. Reliable experimental protocols have been developed for both types of silanization reactions.

Solution-phase silanization. Solution-phase silanization was found to be highly dependent on silane purity and ambient humidity. The impurities in a silane coupling agent may exist in aggregates of aminosilane molecules that attach to a substrate surface via few siloxane bonds, disrupting the regular patterns of silane layers and hence increasing their susceptibility to hydrolysis. Fluctuating ambient humidity could have introduced varied amounts of water to the reaction medium that affected the rate and extent of silanization. Both factors were observed to decrease the reproducibility and hydrolytic stability of

aminosilane-derived layers. The impact of these two factors could be minimized by purifying silane coupling agents prior to solution-phase reactions and using anhydrous non-polar solvents. In addition, silane layers with multilayer characteristics appeared to be more hydrolytically stable and could be obtained by extending reaction time. In general, 24-h solution-phase silanization in anhydrous toluene at 70 °C was found to be sufficient for generating reproducible and hydrolytically stable silane layers with the Group II and III reagents of high purity.

Vapor-phase silanization. Vapor-phase silanization is independent of silane purity since aggregates of aminosilane molecules do not vaporize easily at moderate temperatures and thus they do not react with the substrate surface. The impact of ambient humidity was also minimal due to a consistently drier reaction system in the absence of a solvent. Purging reaction tubes extensively with N₂ was shown to further improve the reproducibility of the experiments. As a result, reproducible aminosilane-derived monolayers are generally easier to obtain in vapor-phase silanization.

As mentioned in the introduction section, recent FT-IR studies challenged the possibility of siloxane bond formation on silicon wafer substrates in vapor-phase silanization. This study demonstrated otherwise. With abundant supporting data, hydrolytically stable aminosilane-derived layers were prepared through vapor-phase reactions, which is consistent with Jonsson *et al's* report³³ on generating smooth, stable, and reproducible silane layers that exhibited monolayer characteristics by the vapor deposition of the Group II reagent AEAPTMS. The

lack of siloxane bond formation reported in the FT-IR studies may be caused by the use of undecanal triethoxysilane (Figure 29). The absence of amine functional groups does not allow the catalysis of siloxane bond formation, similar to our observations with the Group III reagent AHAMTES.

In general, 48-h vapor-phase silanization at 90 °C was shown to be sufficient for generating reproducible and hydrolytically stable silane layers with the Group II reagents.

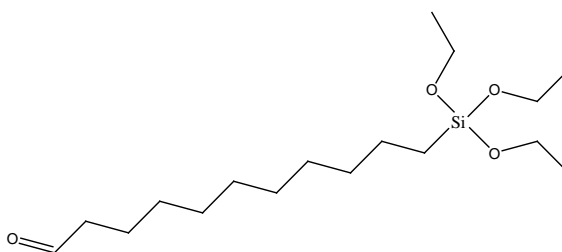


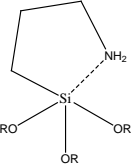
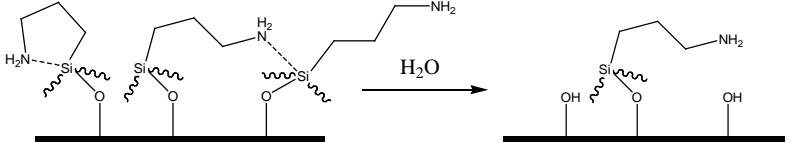
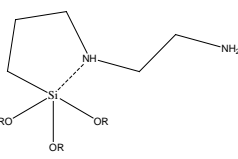
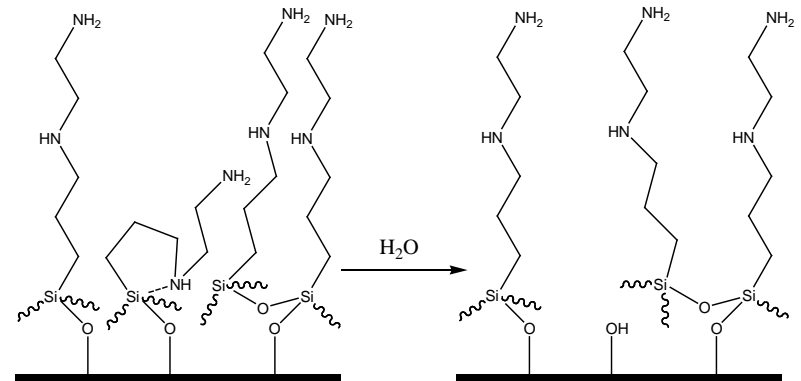
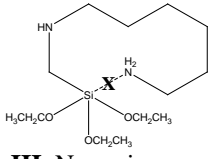
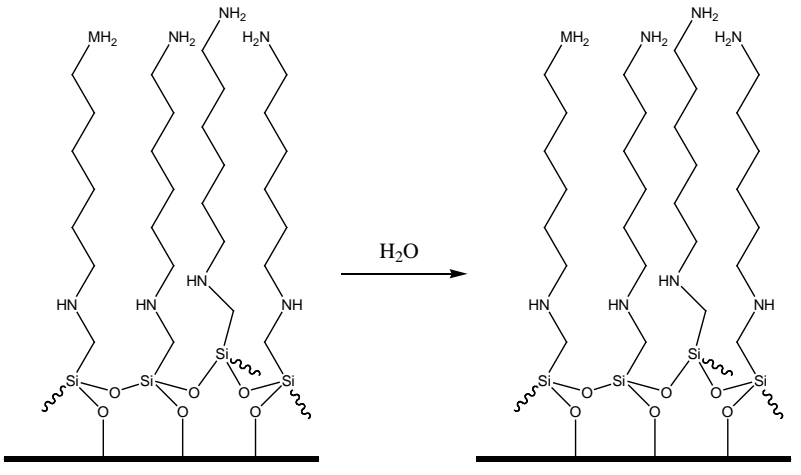
Figure 29. *Molecular structure of triethoxysilyl undecanal.*

Choice of silane coupling agents. As shown in Table 11, Group I reagents, which are the most widely used for current research and applications, tend to produce silane layers with low hydrolytic stability due to the ready occurrence of both intra- and inter-molecularly catalyzed hydrolysis of siloxane bonds. Group II reagents are the most ideal for vapor-phase silanization. Amine catalyzed hydrolysis of siloxane bonds is reduced by increased steric hindrance due to their longer chains. Group III reagents are only suitable for solution-phase silanization since it is incapable of intra-molecular catalysis.

Moreover, tri-ethoxy aminosilanes produce silane layers with higher hydrolytic stability and reproducibility than tri-methoxy aminosilanes since the

reagents with ethoxy groups have lower reactivity and are more forgiving of fluctuating reaction conditions.

Table 11. Hydrolysis schematics of attached silane layers from three different groups.

Group	Hydrolysis
 <p data-bbox="381 709 609 766">I. Primary amine can coordinate to Si</p>	
 <p data-bbox="381 1029 609 1081">II. Secondary amine can coordinate to Si</p>	
 <p data-bbox="397 1501 592 1554">III. No amine can coordinate to Si</p>	

REFERENCES CITED

1. Ulman, A. *Chem. Rev.* **1996**, *96*, 1533.
2. Swalen, J. D.; Allara, D. L.; Andrade, J. D.; Chandross, E. A.; Garoff, S.; Israelachvili, J.; McCarthy, T. J.; Murray, R.; Pease, R. F.; Rabolt, J. F.; Wynne, K. J.; Yu, H. *Langmuir* **1987**, *3*, 932.
3. Love, J. C.; Estroff, L. A.; Kriebel, J. K.; Nuzzo, R. G.; Whitesides, G. W. *Chem. Rev.* **2005**, *105*, 1103.
4. Bigelow, W. C.; Pickett, D. L.; Zisman, W. A. *J. Colloid Interface Sci.* **1946**, *1*, 513.
5. Vuillaume, D.; Boulas, C.; Collet, J. *Appl. Phys. Lett.* **1996**, *69*, 1646.
6. Li, Y. S.; Wang, Y.; Tran, T.; Perkins, A. *Spectrochim. Acta Part A* **2005**, *61*, 3032.
7. Chen, K.; Caldwell, W. B.; Mirkin, C. A. *J. Am. Chem. Soc.* **1993**, *115*, 1193.
8. Choi, J. U.; Lim, C. B.; Kim, J. H.; Chung, T. Y.; Moon, J. H.; Hahn, J. H.; Kim, S. B.; Park, J. W. *Synth. Met.* **1995**, *71*, 1729.
9. Kapur, R.; Rudolph, A. S. *Exp. Cell Res.* **1998**, *244*, 275.
10. Almeida, A. T.; Salvadori, M. C.; Petri, D. F. S. *Langmuir* **2002**, *18*, 6914.
11. Sugimura, H.; Nakagiri, N. *J. Am. Chem. Soc.* **1997**, *119*, 9226.
12. Chang, Y. C.; Frank, C. W. *Langmuir* **1998**, *14*, 326.
13. Emoto, K.; Van Alstine, J. M.; Harris, J. M. *Langmuir* **1998**, *14*, 2722.
14. Kohler, N.; Fryxell, G. E.; Zhang, M. *J. Am. Chem. Soc.* **2004**, *126*, 7206.
15. Emoto, K.; Harris, J. M.; Van Alstine, J. M. *Anal. Chem.* **1996**, *68*, 3751.
16. Malsten, M.; Emoto, K.; Van Alstine, J. M. *J. Colloid Interface Sci.* **1998**, *202*, 507.
17. Miksa, D.; Irish, E. R.; Chen, D.; Composto, R. J.; Eckmann, D. M. *Biomacromolecules* **2006**, *7*, 557.
18. Hu, J.; Wang, M.; Weier, H. U. G.; Frantz, P.; Kolbe, W.; Ogletree, D. F.; Salmeron, M. *Langmuir* **1996**, *12*, 1697.
19. Callow, M. E.; Callow, J. A.; Ista, L. K.; Coleman, S. E.; Nolasco, A. C.; Lopez, G. P. *Appl. Environ. Microbiol.* **2000**, *66*, 3249.
20. Eisenberg, J. L.; Piper, J. L.; Mrksich, M. *Langmuir* **2009**, *25*, 13942.
21. Guo, L. Y.; Zhao, Y. P. *J. Adhes. Sci. Technol.* **2006**, *20*, 1281.
22. Martwiset, S.; Koh, A. E.; Chen, W. *Langmuir* **2006**, *22*, 8192.
23. Smith, E. A.; Chen, W. *Langmuir* **2008**, *24*, 12405.
24. Fadeev, A. Y.; McCarthy, T. J. *Langmuir* **2000**, *16*, 7268.
25. Vandenberg, E. T.; Bertilsson, L.; Liedberg, B.; Uvdal, K.; Erlandsson, R.; Elwing, H.; Lundstron, I. *J. Colloid Interface Sci.* **1991**, *147*, 103.
26. Zhang, F.; Srinivasan, M. P. *Langmuir* **2004**, *20*, 2309.
27. Zhdanov, S. P.; Kosheleva, L. S.; Titova, T. I. *Langmuir* **1987**, *3*, 960.
28. Simon, A.; Cohen-Bouhacina, T.; Porte, M. C.; Aime, J. P.; Baquay, C. J. *J. Colloid Interface Sci.* **2002**, *251*, 278.

29. McGovern, M. E.; Kallury, K. M. R.; Thompson, M. *Langmuir* **1994**, *10*, 3607.
30. Howarter, J. A.; Youngblood, J. P. *Langmuir* **2006**, *22*, 11147.
31. Waddell, T. G.; Leyden, D. E.; DeBello, M. T. *J. Am. Chem. Soc.* **1981**, *103*, 5303.
32. Pasternack, R. M.; Amy, S. R.; Chabal, Y. J. *Langmuir* **2008**, *24*, 12963.
33. Jonsson, U.; Olofsson, G.; Malmqvist, M.; Ronnberg, I. *Thin Solid Films* **1985**, *124*, 117.
34. Fiorilli, S.; Rivolo, P.; Descrovi, E.; Ricciardi, C.; Pasquardini, L.; Lunelli, L.; Vanzetti, L.; Pederzoli, C.; Onida, B.; Garrone, E. *J. Colloid Interface Sci.* **2007**, *12*, 41.
35. Ek, S.; Iiskola, E. I.; Niinisto, L.; Vaittinen, J.; Pakkanen, T. T.; Keranen, J.; Auroux, A. *Langmuir* **2003**, *19*, 10601.
36. Ek, S.; Iiskola, E. I.; Niinisto, L. *Langmuir* **2003**, *19*, 3461.
37. Ek, S.; Iiskola, E. I.; Niinisto, L. *J. Phys. Chem. B* **2004**, *108*, 9650.
38. Tian, R.; Seitz, O., Li, M.; Hu, W.; Chabal, Y. J.; Gao, J. *Langmuir* **2010**, *26*, 4563.
39. Jenkins, Francis A. and Harvey E. White. In *Fundamentals of Optics*; McGraw Hill Inc., New York, **1976**.
40. J.A. Woollam Co., Inc. Ellipsometry Solutions.
<http://www.jawoollam.com> (accessed April 5, 2011).
41. Theoretical Aspects and Instrumentation of Ellipsometry handout.
42. Wikipedia page. http://en.wikipedia.org/wiki/File:Ellipsometry_setup.jpg (accessed April 5, 2011).
43. Young, T. *Philos. Trans. R. Soc. London* **1805**, *95*, 65.
44. Wikipedia page. http://en.wikipedia.org/wiki/File:Contact_angle.svg (accessed April 5, 2011).
45. Smith, E.A. The Hydrolytic Stability of Aminosilane-functionalized Silicon Surfaces. Thesis, Mount Holyoke College, South Hadley, MA, 2008.
46. *Thermo Fisher Scientific page*.
http://www.thermo.com/eThermo/CMA/PDFs/Various/File_9223.pdf (accessed April 5, 2011).
47. Wenzel, R. N. *Ind. Eng. Chem.* **1936**, *28*, 988.
48. Cassie, A. B. D.; Baxter, S. *Trans. Faraday Soc.* **1944**, *40*, 546.
49. Rugar, D.; Hansma, P. *Phys. Today* **1990**.
50. Binnig, G.; Quate, C. F. *Phys. Rev. Lett.* **1986**, *56*, 930.
51. Veeco Metrology Group. Scanning Probe Microscopy Training Notebook **2000**.
52. Hollander, J. M.; Jolly, W. L. *Acc. Chem. Res.* **1970**, *3*, 193.
53. Fadley, C. S. *Prog. Surf. Sci.* **1984**, *16*, 275.
54. Belgian Nuclear Research Center Page.
http://www.sckcen.be/microstructure/Infrastructure/XPS/Infrastructure_XPS.htm (accessed April 5, 2011).